

CONTROLLED DEPOSITION OF STRUCTURED POLYMER FILMS: CHEMICAL
AND RHEOLOGICAL FACTORS IN CHITOSAN FILM FORMATION

A THESIS SUBMITTED TO THE GRADUATE DIVISION OF THE UNIVERSITY
OF HAWAII AT MĀNOA IN PARTIAL FULFILLMENT OF THE REQUIREMENTS
FOR THE DEGREE OF

MASTER OF SCIENCE

IN

CHEMISTRY

MAY 2012

By

Sedef F. Maloy

Thesis Committee:

Michael Cooney, Chairperson
Joseph Jarrett
Philip Williams

Keywords: Chitosan and modified chitosan, polymer films, spread-coat, micellar
structure

ABSTRACT

The technique of spread-coating was utilized to create thin films of chitosan polymer. The effect of deposition rate on film thickness was characterized for solutions of deacetylated and butyl-modified chitosan. For the range of deposition rates analyzed, the relationship between film thickness and increasing deposition rate fell into three distinct regions: an initial inverse relationship, a second linearly increasing relationship, and a final region wherein the film thickness remained constant. Results suggest that film thickness was both controllable and reproducible and that hydrophobic modification of the polymer extends the range over which a linear relationship between film thickness and deposition rate is achieved.

Viscometry and fluorescence spectroscopy were employed to characterize the micellar characteristics of solutions of both deacetylated and butyl-modified chitosan. Deacetylated chitosan solutions possessed more interconnected hydrophobic domains that had more intermolecular micellar characteristics, while butyl-modified chitosan solutions had more intramolecular micellar characteristics and less interconnected hydrophobic domains.

TABLE OF CONTENTS

Abstract.....	ii
List of Figures	iv
List of Tables.....	v
List of Abbreviations	vi
Chapter 1: Introduction to Chitosan Films and Their Application.....	1
General Overview.....	1
Polymer Micellar Structure.....	4
Fluorescence Spectroscopy of Chitosan Polymers.....	9
Enzyme Immobilization.....	10
Thin Film Formation.....	12
Summary	14
Chapter 2: Experimental Methods.....	16
Chemicals.....	16
Preparation of Deacetylated Chitosan	16
Preparation of Butyl-Modified Chitosan	17
Preparation of Chitosan Solutions	17
Preparation of Micron Thin Chitosan Films	18
Measurement of Film Thickness	19
Viscosity Measurements	20
Fluorescence Measurements	21
Solid-State NMR Analysis.....	21
Chapter 3: Reproducibility of Film Thickness via the Spread-Coating Method	23
Introduction.....	23
Solid-State ¹³ C NMR of Deacetylated and Butyl-Modified Chitosan.....	23
The Air-Drying Method and Substrate Properties	26
Impact of the Razor Blade Incision on Film Thickness	28
Reproducibility of the Film Thickness and the Microscope.....	32
Chapter 4: Film Thickness vs. Deposition Rate of Spread-Coat Chitosan Films	37
Introduction.....	37
Deacetylated Chitosan Films.....	37
Butyl-Modified Chitosan Films.....	42
Chapter 5: Solution Micellar Characteristics via Viscosity and Fluorescence	47
Introduction.....	47
Viscosity of Chitosan Solutions	47
Fluorescence Spectroscopy of Chitosan Solutions.....	51
Chapter 6: Conclusions and Future Directions	58
Conclusions and Summary.....	58
Future Directions	60
References.....	62

LIST OF TABLES

Table 1. Incisions on Blank Slide with Differing Applied Pressure	29
Table 2. Instrument Precision and Reproducibility.....	33
Table 3. Thickness of 2% (w/w) Deacetylated Chitosan Films at Deposition Rate of 20 cm/hr	34
Table 4. Thickness of 2% (w/w) Deacetylated Chitosan Films at Deposition Rate of 2 cm/hr	34
Table 5. Deposition Rate vs. Film Thickness of 2% (w/w) Deacetylated Chitosan	38
Table 6. Deposition Rate vs. Film Thickness of 2% (w/w) Butyl-Modified Chitosan ...	44
Table 7. Viscosity vs. Chitosan Concentration	49
Table 8. I ₁ /I ₃ Ratios for Chitosan Solutions.....	54

LIST OF FIGURES

Figure 1. Reaction Scheme of Chitin to Chitosan and Hydrophobically Modified Chitosan	3
Figure 2. Schematic of Film Deposition.....	13
Figure 3. Solid-State ¹³ C NMR Spectra of Deacetylated and Butyl-Modified Chitosan	25
Figure 4. Images from the Keyence microscope.....	31
Figure 5. Reproducibility of Film Thickness	35
Figure 6. Film Thickness vs. Deposition Rate of 2% (w/w) Deacetylated Chitosan for 3 Sets of Films	38
Figure 7. Film Thickness vs. Deposition Rate of 2% (w/w) Deacetylated Chitosan with Trends	39
Figure 8. Film Thickness vs. Deposition Rate of 2% (w/w) Butyl-Modified Chitosan for 3 Sets of Films.....	43
Figure 9. Film Thickness vs. Deposition Rate of 2% (w/w) Butyl-Modified Chitosan with Trends.....	45
Figure 10. Viscosity vs. Chitosan Concentration.....	48
Figure 11. Fluorescence Emission Spectra of Deacetylated Chitosan	52
Figure 12. Fluorescence Emission Spectra of Butyl-Modified Chitosan	53
Figure 13. Polarity Parameter (I ₁ /I ₃) vs. Chitosan Concentration.....	55

LIST OF ABBREVIATIONS

C	Celsius
cm	Centimeter
cP	Centipoise
CPMAS	Cross-Polarization Magic Angle Spinning
g	Gram
hr	Hour
I_1/I_3	Intensity Ratio of the First and Third Vibronic Energy Bands
kDa	Kilodaltons
kHz	Kilohertz
L	Liter
M	Molarity
mg	Milligram
MHz	Megahertz
mL	Milliliter
nm	Nanometer
NMR	Nuclear Magnetic Resonance
pH	Negative Common Logarithm of Hydronium Ion Concentration
pKa	Negative Common Logarithm of Acid Dissociation Constant
ppm	Parts per Million
psi	Pounds per Square Inch
RPM	Revolutions per Minute
σ	Standard deviation

VLP	Virus-Like Particles
(v/v)	Concentration in Volume Ratio
(w/v)	Concentration in Mass/Volume Ratio
(w/w)	Concentration in Mass Ratio
\bar{x}	Average Measured Thickness
2-D	Two-Dimensional
3-D	Three-Dimensional
μL	Microliter
μM	Micromolar
μm	Micrometer
[]	Concentration
°	Degree
#	Number
%	Percent

CHAPTER 1:

INTRODUCTION TO CHITOSAN FILMS AND THEIR APPLICATION

GENERAL OVERVIEW

Chitosan polymer has gained attention in the research community over the past few decades, in part because of its ability to be blended with other biomaterials and/or molded into highly porous matrices, creating great potential as a biomaterial for enzyme immobilization, drug delivery, and gene delivery.¹⁻³ Because of chitosan's demonstrated ability to immobilize enzymes in scaffold electrodes^{1,2,4} and to provide enzyme stabilizing chemical microenvironments,^{1,2,4-9} new information regarding the utility of the spread-coating technique to fabricate micron thin chitosan biopolymer films, in terms of its ability to control film thickness and morphology, could prove of great benefit with regards to the field of enzyme immobilization and the production of chitosan-based biofuel cell electrodes and biosensors.

Biofuel cells are very promising as potential energy-generating systems due to their relatively inexpensive assembly. However, there are a few obstacles that must be overcome before they become applicable. The main issues faced by biofuel cells are short lifetimes and low power density.¹⁰ These factors are mainly controlled by the enzyme stability, electron transfer rate, and enzyme loading.¹⁰ Enzyme immobilization has thus become a key area of study for improving the performance of biofuel cells.

An ideal material for enzyme immobilization would be conductive, porous, and have a large surface area. These properties allow for better kinetics of the electron transfer and higher enzyme incorporation. Nafion is currently the archetype material for

enzyme immobilization in biofuel cell membranes. It has been demonstrated by Minteer et al., 2004 that an ethanol/O₂ biofuel cell can generate considerable power densities using entrapment of select NAD⁺-dependent dehydrogenases (alcohol, aldehyde, glucose, and lactic dehydrogenases) in a tetraalkylammonium bromide modified Nafion membrane.^{10,11} Although Nafion is capable of immobilizing a variety of enzymes, it is expensive and lacks biocompatibility and biodegradability.⁵ Chitosan is, therefore, an ideal alternative to Nafion as it is less expensive, biodegradable and has better biocompatibility.

Chitosan is a deacetylated derivative of chitin, β -(1 \rightarrow 4') linked 2-acetamido-2-deoxy-D-glucose, found largely in the exoskeletons of crustaceans and insects and in cell walls of fungi. Chitin is the second most abundant, naturally produced polysaccharide; making it ideal for commercial applications, as cost efficiency is always a critical concern, as well as biocompatibility, biodegradability, and non-toxicity.¹² Chitin is commercially obtained as a waste product of the canning industry in the form of crab and shrimp shells, lending to its economic practicality.¹² Chitin can readily be deacetylated, where having less than about 40% of the monomers retaining the acyl moiety indicates the transition from chitin to the chitosan polymer. Chitosan is a random copolymer, possessing two monomer units; glucosamine and *N*-acetylglucosamine, where the location of the remaining *N*-acyl functional groups is random.

The solubility of chitosan is very limited to mildly acidic conditions, as strong acid will cause rapid polymer degradation. Furthermore, only certain acids are capable of solubilizing the polymer, such as the acid primarily utilized in this study, acetic acid. The ammonium cation on the polymer backbone has a pKa of approximately 6.5,^{13,14}

indicating that in solutions of acetic acid, which has a pKa of 4.76, the amine is protonated and has a formal positive charge. The ionization of the amine renders chitosan a polyelectrolyte, making it a feasible material for applications in biofuel cells and biosensors as a conducting membrane or scaffold. The polyelectrolytic behavior of the amine moiety dictates that the solution conformation would be somewhat linear as the ionic groups would repel each other.

The presence of the amine group also allows chitosan to be further functionalized, thereby varying its properties and applicability. For example, deacetylated chitosan can be chemically modified to introduce amphiphilic micellar structure.^{5-9,15,16} Introduction of an *N*-alkyl moiety on the water/acid soluble, hydrophilic polymer backbone yields a hydrophobic side chain, making the polymer amphiphilic, a characteristic that allows micellar structure or soluble aggregates to form. Evidence for the formation of micellar regions in chitosan have been detected via transmission electron microscopy, fluorescence spectroscopy, and static and dynamic light scattering experiments.^{3,5,15,17} Figure 1 shows the reaction scheme of chitin to deacetylated chitosan and hydrophobically modified chitosan.

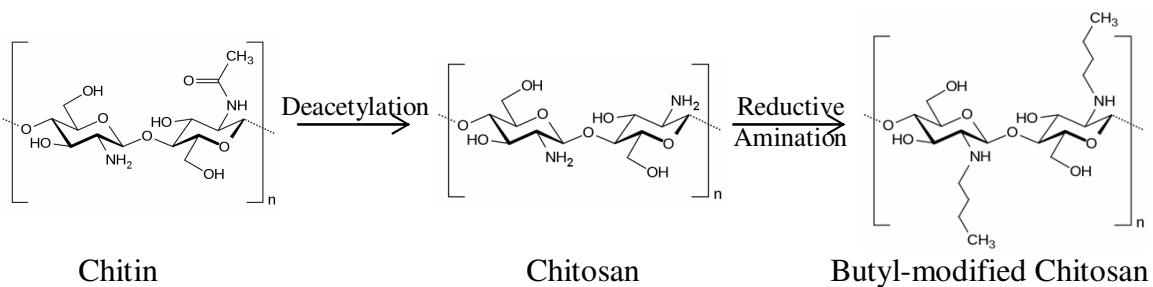


Figure 1. Reaction scheme of chitin to chitosan through deacetylation and of chitosan to hydrophobically modified chitosan through reductive amination.

In this scenario, hydrocarbon chains are substituted onto the hydrophilic polyelectrolyte backbone through reductive amination reactions, prepared in acidic media. The reaction of an aldehyde with the amine moiety results in the formation of an imine, followed by the selective reduction using sodium cyanoborohydride as the reducing agent. Due to the aqueous nature of the reaction solution, vigorous stirring is necessary upon addition of the aldehyde and the reducing agent in order for the aqueous polymer to come in contact with the organic reagent.⁹ These reductive amination reactions yield a hydrophobically modified polymer possessing solution-based intra- and intermolecular micellar structure that has been shown to improve enzyme catalytic activity, stability, and active lifetime when molded into air-dried films.^{1,2,4-9} Less understood, but no less important, is the question of how the presence of solution-based intra- and intermolecular micellar structure impacts the final thickness and morphology of the films.

POLYMER MICELLAR STRUCTURE

In order to apply the spread-coating technique to the deposition of chitosan films, it is important to understand the underlying chemical interactions involved regarding amphiphilic polymers, such as chitosan, as it will directly affect the film deposition mechanisms and the resulting air-dried films. Solutions of amphiphilic polymers above a certain concentration, called the critical micelle concentration, will self-aggregate as a consequence of their hydrophobic moieties forming hydrophobic domains, thus leading to formation of “micelles” associated with folding and partial self-aggregation of the polymer domains. Micelle formation depends largely on the hydrophobic effect, which is

driven by the entropy involved in the solvation of hydrophobic molecules in water. If the hydrophobic molecules have a larger the surface area, then the solvation shell surrounding them must be larger. This shell requires the water molecules to be ordered around the hydrophobic molecules and is entropically unfavorable. Aggregation of the hydrophobic molecules into micelles minimizes the surface area, thereby increasing the entropy of the system.

Chitosan polymer can be hydrophobically modified to exhibit such amphiphilic properties when dissolved in acidic aqueous solutions, forming a dynamic equilibrium of micellar aggregates that vary in size, interconnectivity and their capacity to stabilize enzymes.⁵⁻⁹ Although the formation of micelles depends on entropy, the structure of the micellar regions of chitosan solutions depends on the relative amounts of intra- and intermolecular chemical/electronic interactions as well as key process variables, such as polymer concentration.^{3,5,6,15,16} These chemical interactions include hydrogen bonding which occurs between the hydroxyl functional groups of the polymer backbone within a particular polymer strand, between neighboring strands, and with water molecules in the solution. Hydrogen bonding and electrostatic repulsions of the polyelectrolytic backbone, along with van der Waals dispersion forces that are present between all molecules, provides the attractive and repulsive interactions that are responsible for the differences in amounts of intra- and intermolecular aggregation of the hydrophobic side chains along the chitosan backbone. Although these forces are largely responsible for the formation of intra- and intermolecular micelles in solution and impact the resulting thickness of thin films made from these solutions, the polymer concentration will influence the relative

dominance of intra- to intermolecular interactions in solution, and thus potentially influence the thickness and morphology of thin films made from these solutions.

The effect of polymer concentration on micellar characteristics, such as size, number, and concentration of unimolecular micelles (micelles comprised of a single polymer strand, i.e., only intramolecular aggregation) and micellar aggregates, has been extensively reported by Esquenet et al., 2001 for solutions of medium molecular weight hydrophobically modified chitosan (i.e., 190-310 kDa).^{15,16} Specifically, the process of hydrophobic side chain aggregation was categorized into three distinct concentration dependent phases that differed in their rheological and micellar properties: (i) a supernatant phase comprising intramolecular interactions that formed unimolecular micelles, (ii) a micellar phase primarily comprising both intra- and intermolecular forces, and (iii) an associative gel phase dominated by intermolecular interactions, which accounted for a large increase in viscosity relative to the supernatant and micellar phases.¹⁵ In follow-up work, Esquenet et al., 2004 extended these descriptions to describe a fourth category as a phase separation between the polymer and the aqueous phase.¹⁶ Although these works provide insight into the use of solution concentration to control and manipulate the solution-based intra- and intermolecular micellar structure of hydrophobically modified chitosan, they should not be taken to suggest that solution concentration is the only process variable that could impact the solution based inter- and intramolecular micellar structure. For instance, the length and degree of hydrophobic substitution along the chitosan backbone are also, if not equally, important to intra- and intermolecular micellar structure.^{3,5,6,15,16}

Klotzbach et al., 2006 suggested that the optimal length of the hydrophobic side chain should contain between 4 and 10 carbons, proposing that if the length of the side chain becomes too large, the number of micellar domains will decrease but the size of the domains will increase.⁵ By contrast, if the length of the side chain is too small or nonexistent, micellar structure within the polymer strands will not form.^{5,9} Similarly, the degree of hydrophobic substitution can become too low to catalyze inter- or intramolecular hydrophobic aggregation, or it can become so large that hydrophobic properties will dominate the interactions and the polymer will become insoluble in aqueous solutions.³ Although independently, these variables have the aforementioned effects, when combined, they can be carefully balanced to manipulate the resultant micellar structure. For example, with long alkyl chains and a low degree of substitution, or conversely, with short alkyl chains and a high degree of substitution it is still possible to see aggregation, though they will be very different in their relative degree of intra- vs. intermolecular interactions. However, long alkyl chains and a high degree of substitution will render the polymer insoluble in aqueous solutions due to the increased hydrophobic nature of the polymer, while short alkyl chains and a low degree of substitution will not encourage aggregation due to a lack of hydrophobicity.

Another important consequence of the degree of substitution is the micellar structure of polymer strands. A low degree of hydrophobic substitution, i.e., 2% in both previous cases by Esquenet and Buhler, 2001 and Esquenet et al., 2004, yielded an abundance of looped structures along the chitosan backbone.^{15,16} This occurred because the distance between each hydrophobic group was great enough to allow the hydrophobic functional groups (i.e., side chains) along the polymer backbone to aggregate, forming

loops. Therefore, a low degree of substitution promotes intramolecular aggregation, while a high degree of substitution increases the amount of intermolecular aggregation. Also, it is important to note that the degree of substitution is related to the degree of deacetylation of the polymer, as only deacetylated monomers can be further modified to incorporate an alkyl chain.

Commercially produced chitosan varies greatly from batch to batch, including the degree of deacetylation and the length of the polymer itself, revealing a significant source of experimental error with regards to the micellar structure. As such, the batch of chitosan used should be the same for all experiments and should be uniformly modified. For instance, the deacetylation procedure calls for harsh reaction conditions, such as a highly concentrated, strongly basic solution, which does not allow for a homogenous reaction medium and can lead to partial degradation of the polymer.^{9,18,19} Likewise, solution heterogeneity can be problematic during the *N*-alkylation process, as well as the extent of the reaction, regioselectivity, and structural ambiguity of the products.¹² It may be possible to gain some level of control over the variation in batches if the polymer is almost fully deacetylated via autoclaving under strongly basic conditions, followed by chromatographic separation by polymer chain length prior to use for a set of experiments. Since there are many factors that can contribute to the micellar structure of chitosan polymer solutions that arise based on the batch of chitosan and the modification procedures, it is essential to control these parameters to determine how these aspects affect the micellar structure of any given chitosan solution and, ultimately, the films prepared from them.

FLUORESCENCE SPECTROSCOPY OF CHITOSAN POLYMERS

Fluorescence spectroscopy can and has been utilized in the study of hydrophobic regions of amphiphilic polymers, including chitosan. When incorporated into the micellar regions of an amphiphilic polymer, a hydrophobic fluorescent probe will exhibit an emission spectrum indicative of its chemical microenvironment. Although chitosan polymers have been examined using this technique, due to the complexity of chemical interactions and variety that arises from even slight variations in preparation methods, it is necessary and informative to study chitosan solutions intended for film deposition.

Although the literature is in agreement regarding the presence of unimolecular micelles and micellar aggregates in solutions of hydrophobically modified chitosan, slightly conflicting evidence has been reported by Philippova et al., 2001, Klotzbach et al., 2006, and Martin et al., 2009 regarding the presence of hydrophobic domains in solutions of deacetylated chitosan.^{5,8,20} Fluorescence spectroscopy has been used to characterize the hydrophobicity of solutions of native and modified chitosan, however, each used a different probe. Using pyrene, Philippova et al., 2001 observed hydrophobic domains in solutions of unmodified chitosan but at higher concentrations than the hydrophobically modified analogues, a feature attributed to a compacted structure of the aggregates or a small amount of polymer chains participating in aggregation.²⁰ In this case, the chitosan polymer studied was 88% deacetylated with 4% substitution of dodecyl chains for the modified analogue. To support this evidence, viscosity measurements were taken for the chitosan polymers, which showed that both modified and unmodified chitosan experience an exponential increase in solution viscosity as a function of concentration, but the unmodified chitosan did so at higher concentrations. According to

Martin et al., 2009 using 1-anilino-8-naphthalene sulfonate (ANS) as the probe, emission intensities of solutions of deacetylated and hydrophobically modified chitosan suggested that deacetylated chitosan does not exhibit hydrophobic domains.⁸ Although, in this case, *N*-alkyl chain lengths examined were butyl and octyl groups and a fluorescent probe with different chemical properties was used. Their results showed that the chemical microenvironment of ANS in solution with unmodified chitosan was very similar to that of acetic acid, suggesting that the fluorophore was not incorporated into hydrophobic domains. Likewise, using fluorescence microscopy with fluorescein and Ru(bpy)₃²⁺ as probes, Klotzbach et al., 2006 were also unable to detect hydrophobic domains in unmodified chitosan.⁵ As such, a uniformly supported theory of when and how inter- and intramolecular micellar structures form in solutions of hydrophobically modified and deacetylated chitosan remains unclear, as well as whether or not the micelles will remain intact through the evaporation process.

ENZYME IMMOBILIZATION

Chitosan has demonstrated the ability to immobilize enzymes while improving catalytic activity, stability, and active lifetime.^{1,2,4-9} These improvements are likely due to the biocompatibility of chitosan polymer. Traditional methods of enzyme immobilization include cross-linking, encapsulation, entrapment, and adsorption. In order for an enzyme to be immobilized in chitosan, it must be stable against denaturation throughout the immobilization procedure, which includes exposure to acidic solutions. The ability to vary the pore size of chitosan-based materials¹ allows for the incorporation of enzymes of varying size. Once immobilized on a solid substrate, the chitosan/enzyme matrix can be

utilized in biofuel cell electrodes, biosensors, etc. Enzymes intended for use in a catalytic cycle may be immobilized on a solid substrate for a variety of reasons. One such advantage is the ability to control the extent of an enzymatic reaction in terms of duration of the reaction, loss of enzymes in the product, and amount of enzyme and substrate used.¹² If the enzyme were in solution, the enzyme would be lost as the product is isolated, resulting in a need for more enzyme to extend the catalytic cycle. This would detract from control over how much enzyme is used in the reaction. In contrast, an immobilized enzyme can be continuously separated from product in a flow through device. In addition, an immobilized enzyme can be easily removed in order to stop the reaction after any desired amount of time. These advantages refer to ideal immobilization and require the process of immobilization to be reproducible, which can be problematic in the case of chitosan unless a standardized, uniform starting material is used.

The discussions above reference the presence of unimolecular micelles and micellar aggregates in solutions of native or modified chitosan polymer.^{3,5,6,8,15,16,21,22} This is important from the perspective that for deacetylated chitosan, an enzyme is not immobilized while in solution and in the presence of the polymer (i.e., via encapsulation), but rather while the polymer condenses around the enzyme into a solid film either through freeze or air-drying (i.e., via entrapment).⁷ However, upon phase separation, hydrophobically modified chitosan shows an increase in enzyme retention in the scaffold compared to deacetylated chitosan, suggesting that increased retention is related to an interaction between the enzymes and the hydrophobic groups in solution (i.e., via encapsulation).⁷ These findings seem rather contradictory and unexpected, especially in light of the fact that the enzymes are assumed to prefer an aqueous environment. One

possible explanation could be that the polar units are on the outside and inside of the micellar regions, with the hydrophobic groups in between them, much like a lipid bilayer, and the enzyme is on the inside surrounded by a shell of polar moieties. Although it has been reported for low molecular weight polymers and copolymers that a collapse of the intermolecular micellar structure is induced by an ordering of the crystal structure during the evaporative drying process,^{3,23} the relevance of these findings to larger molecular weight polymers, such as chitosan, remains poorly understood. Consequently, a characterization of how the presence and relative concentration of solution-based unimolecular micelles and/or micellar aggregates could impact the final thickness and morphology of air-dried films for medium molecular weight deacetylated or hydrophobically modified chitosan polymer is fundamental to the advancement of chitosan polymer as an immobilization material.

THIN FILM FORMATION

To help isolate the impact of chemical modification on film thickness, the method used to fabricate and dry the thin films should introduce relatively mild forces. There are several deposition methods available to fabricate air-dried thin films, including spin-coating, dip-coating and spread-coating, each providing different levels of controllability over the film's final morphology and imparting varying degrees of force. The forces that arise from the air-drying method, introduced by evaporation of water from a thin layer of mostly aqueous solution, are unlikely to dominate over the forces provided by the micellar structure. One limitation to air-dried films, however, is the uneven coating thickness that can arise from simple deposition techniques, such as dip-coating. Although

spin-coating can be used to create micron thin films of uniform thickness, this technology imparts severe gradients that could modify the polymer micellar structure. By contrast, the method of spread-coating, shown in Figure 2, can deposit films that are thinner than can be achieved via spin- or dip-coating and in a manner that is both reproducible and absent of the influence of strong external forces.²⁴

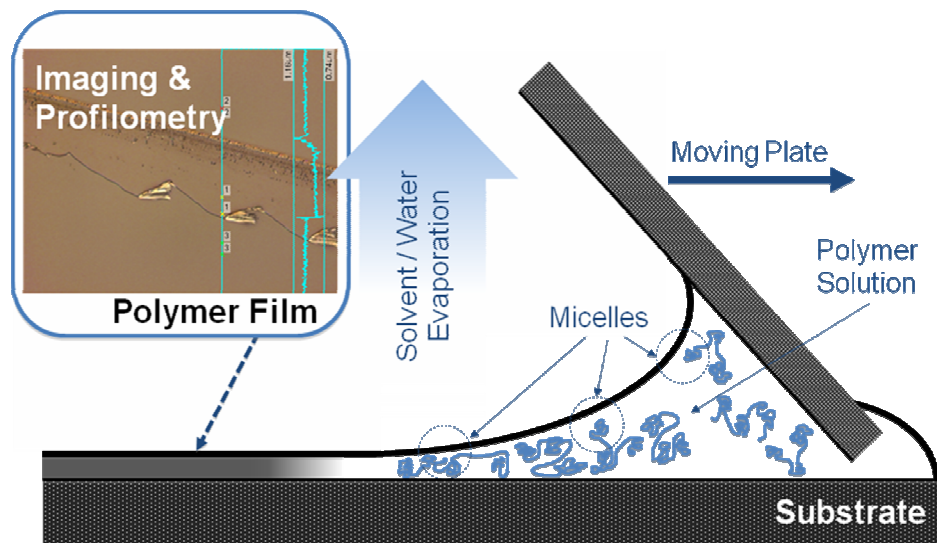


Figure 2. Schematic of film deposition with inlayed microscope image from thickness measurement of air-dried film (top left). Deacetylated or butyl-modified chitosan solutions were pipetted on the obtuse side of the intersection of the two glass slides held at an angle of $30 \pm 1^\circ$. A meniscus forms under the leading slide as it pushes against the solution droplet and across the lower glass substrate at a constant velocity, leaving a thin layer of solution behind. Films formed as the solution was air-dried.

Spread-coating was first introduced as a method for convective self-assembly of colloidal particles.²⁵ The spread-coating technique can be used not only in forming particles or macromolecular assemblies, but also in controlled deposition of thin films. Yuan et al., 2006 used spread-coating for evaporation induced convective assembly in sol-gel derived silica films.²⁴ In an extension of this work, Yuan et al., 2007 used spread-coating as an evaporation driven self-assembly method to form ferritin monolayers on solid substrates, such as silicon wafers and glass microscope slides.²⁶ Both examples

were found to correlate the velocity of solution deposition to other parameters such as the porosity, thickness, volume fraction of particles in solution, and convection forces. Most recently, this technique was used to demonstrate the formation of 2-D structures by assembly of virus-like particles (VLP).²⁷ The spread-coating technique has also been used in the controlled deposition of thin films through evaporation induced convective assembly in sol-gel derived silica films.²⁴ Mesoporous silica films of thickness lower than 100 nm were obtained, exhibiting the micellar (lamellar) structure of the templated surfactant.²⁴ Spread-coating has also been employed in the fabrication of thin films of mesoporous silica and ferritin films for application in photo-responsive materials, membrane base separation, catalysis, electrochemical biosensors, electronics, and optics.^{24,26,28}

Extending this technique towards the fabrication of micron scale or sub-micron thin organic polymer films presents a new challenge. For this application it is critical to establish parameters, under which the self-assembly of hydrophilic and hydrophobic domains of such polymers occurs at the time-scale of the coating deposition. As such, formation of films consisting of deacetylated and hydrophobically modified chitosan biopolymer presents an opportunity in which such assembly of polymer with micellar structures can be established.

SUMMARY

This work extends these developments to the spread-coating of micron thin chitosan films, specifically regarding the impact of solution based micelle structure (gained through the introduction of hydrophobic modification of chitosan polymer) on

film thickness and morphology. Additional knowledge is derived from investigating the correlation between the deposition rate and the final thickness of the spread-coated polymer films. Having the ability to understand how hydrophobic modification, used to introduce solution-based micelle structure and micellar aggregates, affects the film thickness and morphology when used to fabricate micron thin films, will provide additional technological capability supporting the development biofuel cells and biosensors using polymers capable of enzyme immobilization.

CHAPTER 2:

EXPERIMENTAL METHODS

CHEMICALS

Medium molecular weight chitosan (Sigma-Aldrich, 448877), glacial acetic acid (Fisher Scientific, A38^C-212), methanol (Fisher Scientific, A412-4), butyraldehyde (Sigma-Aldrich, 538191-1L, dry, 99%), sodium cyanoborohydride (Fluka, 71435), sodium hydroxide (Fisher Scientific, S318-3), 1-pyrenebutanoic acid (Molecular Probes, P32), and toluene (Fisher Scientific, T324-500) were used as purchased unless otherwise noted.

PREPARATION OF DEACETYLATED CHITOSAN

Prior to use, the native chitosan powder was deacetylated to approximately 95%, according to the procedures of Sjöholm et al., 2009.⁹ Specifically, chitosan powder was mixed with 45% (w/w) sodium hydroxide to a final ratio 1:15 (w/v), followed by autoclaving in a high pressure steam sterilizer (Tomy, ES-315) for 20 minutes at 121°C and 15 psi. Once the solution cooled to room temperature, the chitosan powder was filtered out of solution using coarse micron filter paper (Whatman, 1004-110) and washed with excess deionized water until the filtrate tested neutral with pH indicator strips (EMD colorpHast 0-14 pH, 9590), followed by washing with 100 mL methanol, dried under vacuum at 60°C until dry, and stored under desiccation until used.

PREPARATION OF BUTYL-MODIFIED CHITOSAN

Deacetylated chitosan powder was hydrophobically modified by covalent binding of butyraldehyde to the free amine groups along the chitosan backbone (i.e., reductive amination), according to the procedure of Cooney et al., 2008.¹ The carbonyl group on butyraldehyde reacts with the amine group on chitosan to form an imine, which is then reduced to an amine by sodium cyanoborohydride, with the resulting ratio of chitosan to butyl groups reaching approximately 1:1, as determined by peak integration values using NMR spectroscopy. Specifically, 2 g batches of deacetylated chitosan were dissolved in 60 mL of 1% (v/v) acetic acid under rapid stirring, forming a viscous gel-like solution, followed by the addition of 60 mL of methanol. After continuous stirring for 15 minutes, 80 mL of butyraldehyde were added to the solution along with 5 g of sodium cyanoborohydride. This solution was then stirred and allowed to return to room temperature, upon which time the white precipitate was vacuum filtered and washed with two 100 mL increments of methanol, 100 mL of water, and 100 mL of methanol. A flakey white solid was obtained after drying in a vacuum oven until dry at 60°C. The batches of flaky crystals were combined, crushed, washed again with three 100 mL increments of water and two 100 mL increments of methanol, and placed in a vacuum oven at 60°C until dry. Once dry, the chitosan powder was stored under desiccation.

PREPARATION OF CHITOSAN SOLUTIONS

Solutions of 2% (w/w) deacetylated or butyl-modified chitosan were prepared 24 hours prior to use by dissolving the washed and dried chitosan powder in 0.5 M acetic acid. To ensure complete mixing, the chitosan solution was placed in an Ultrasonic

Cleaner (Branson, 3510) for at least one hour then mixed at low agitation, under seal, until used to prepare films.

PREPARATION OF MICRON THIN CHITOSAN FILMS

Prior to film deposition, all glass slides (Corning, 2947-3x1) used for film deposition were pre-cleaned with piranha solution. Caution should be used in the handling and disposal of piranha solution, as it is very dangerous (caustic and explosive) due to its strongly acidic and oxidizing nature. Specifically, 30% hydrogen peroxide was slowly added to concentrated sulfuric acid in a volumetric ratio of 1:3, respectively. Glass substrates were immersed in the solution for at least 1 minute before rinsing well with deionized water and placing under a Class II Biological Safety Cabinet (The Baker Company, SG403) to dry. The dried slides were then stored under desiccation for at least 24 hours, until film deposition.

Micron thin chitosan films were prepared from solutions of 2% (w/w) deacetylated chitosan using a single-syringe infusion pump (Cole-Parmer, EW-74900-00) modified to work as a moving wedge apparatus, as described in Yuan et al., 2006.²⁴ For each film, 20 μ L aliquots were pipetted precisely at the intersection of two glass slides, one lying planar and the second lying inclined at a $30 \pm 1^\circ$ angle, with the solution deposited on the obtuse side of the wedge. The film was deposited by action of the inclined slide moving forward, at a defined velocity, pushing over the chitosan solution. The rate of deposition (i.e., the rate at which the top slide was moved forward) was controlled by action of the modified syringe pump, reconfigured to push the top slide forward, over the lower slide, at a constant rate, as shown in Figure 2. To minimize

evaporation during the film deposition process, the deposition of each film was executed in a Controlled Atmosphere Chamber (PlasLabs, 855-AC) at room temperature, under atmospheric pressure and water saturated air (Air King, 9915). Upon completion of solution deposition, films to be air-dried were immediately removed and stored in a desiccator to dry (at least 24 hours) until further analysis.

MEASUREMENT OF FILM THICKNESS

Films to be analyzed were removed from desiccation and immediately sliced perpendicularly with a razor blade to create a stepwise drop in the film that extended to the glass surface. Three-dimensional topographical images of this region were obtained using a Color 3-D Laser Scanning Microscope (Keyence, VK-8710) at a magnification of 100x. The microscope uses two light sources, laser and white light, to measure the distance and color of the object of analysis by focusing the laser in the x-y plane (plane of the film) while scanning the laser in the z-direction (perpendicular to the plane of the film), which changes the distance between the lens and the film. Height information is obtained by detection of the peak laser light intensity reflected back to the microscope, while color information is gathered from the reflection of the white light at the peak intensity. The surface morphology and thickness for each film was characterized using Surface Contour Imaging Software (Keyence VK Analyzer, 1.2.0.2). Film thickness was estimated by the difference between the film surface and the glass slide, where the surface of the films was measured by the height of the remaining dried chitosan polymer on the glass slide. For each film made, a minimum of 10 thickness measurements were

taken to determine the average measured thickness, \bar{x} , and standard deviations, σ , according to the following equations:

$$\bar{x} = \frac{\sum_{i=1}^n x_i}{n} \quad (1)$$

$$\sigma = \sqrt{\frac{\sum_{i=1}^n (x_i - \bar{x})^2}{n}} \quad (2)$$

The deposition rates were plotted against the thicknesses and statistical analysis performed to determine and quantify their correlation.

VISCOSITY MEASUREMENTS

Deacetylated and butyl-modified chitosan solutions of concentrations ranging from 3.0% to 0.0% (w/w) were prepared in stepwise increments. After 24 hours from the initial preparation of 3.0% (w/w) deacetylated/butyl-modified chitosan in 0.5 M acetic acid, the viscosity was measured, followed by a series of dilutions to obtain each incremental concentration. Upon dilution, the solutions were sonicated for at least one hour and stirred overnight before taking viscosity measurements. A blank was also prepared that contained only 0.5 M acetic acid to represent the 0.0% concentration. The viscosity of these solutions were measured 24 hours after preparation or dilution using a Brookfield Digital Viscometer (LVDV-E) with the guard leg and spindles 61 or 62 attached, rotating at the appropriate corresponding rate between 4 to 100 RPM for 15 minutes. As the spindle rotates in the solution at a known speed, the instrument measures the torque applied to the spindle and correlates this to the solution viscosity. The viscosity of the 500 mL solutions in a 600 mL low-form beaker were measured at 25°C

in triplicate for each concentration of both deacetylated and butyl-modified chitosan solutions and the results plotted against solution concentration.

FLUORESCENCE MEASUREMENTS

Steady state fluorescent measurements were recorded using a Photon Counting Spectrofluorometer (ISS, PC1) and the data analyzed with the provided software (ISS Vinci, 1.6.SP7). For all sample solutions, 0.8 μM 1-pyrenebutanoic acid was used as a fluorescent probe. Fluorescence emissions were recorded for 3 mL solutions of deacetylated and butyl-modified chitosan, prepared 24 hours in advance, ranging in concentrations from 0.0% to 3.0% (w/w). Standard solutions were also prepared containing water, toluene, or 0.5 M acetic acid. The intensity ratio of the first and third vibronic energy bands was plotted against the solution concentration to determine the probe's chemical microenvironment.

SOLID-STATE NMR ANALYSIS

Spectra for chitosan samples were recorded in the solid-state using Cross-Polarization Magic Angle Spinning (CPMAS) ^{13}C NMR experiments. Approximately 30 to 40 mg, dry weight, of deacetylated or butyl-modified chitosan was removed from desiccation, placed in a sample tube, and the proton decoupled ^{13}C spectra were acquired (Varian: Unity Inova 400 WB (Oxford magnet)) at a frequency of 100.583 MHz and 399.973 MHz for ^{13}C and ^1H , respectively. The samples were spun at a rotation speed of 8 kHz (for ^{13}C and ^1H) and an angle of 54.7° (the magic angle). Hexamethylbenzene was

used as a reference for the chemical shifts with the methyl carbons set to 17.00 ppm (the chemical shift of the carbons on the benzene ring was 131.98 ppm).

CHAPTER 3:
REPRODUCIBILITY OF FILM THICKNESS VIA THE SPREAD-COATING
METHOD

INTRODUCTION

Reproducibility is important in advancing a technology such as the generation of chitosan thin films for use in enzyme immobilization from research to application. Previous studies using the spread-coating method have shown that reproducible films can be prepared using silica, ferritin, and virus-like particles.^{24,26,27} A study into the reproducibility of the thickness of chitosan films produced by the spread-coating method was undertaken with the goal of creating a standard procedure for the consistent production of micron thin chitosan films. In order to carry out this study, it was necessary to determine the reproducibility of the methods chosen to produce films and the analytical techniques used to measure their thickness. Specifically, the method for spread-coating the chitosan films, the precision of the microscope, and the effect of the incision made in the films on the thickness measurement were investigated. Also, verification of the uniformity of deacetylation and butyl-modification of chitosan was obtained using NMR.

SOLID-STATE ¹³C NMR OF DEACETYLATED AND BUTYL-MODIFIED CHITOSAN

In the interest of preparing chitosan films that are reproducible and comparable, all deacetylated chitosan films were prepared from a single batch of deacetylated

chitosan, some of which was then hydrophobically modified to incorporate the butyl side chain and used to prepare all butyl-modified films. Solid-state cross-polarization ^{13}C NMR experiments on the deacetylated and butyl-modified chitosan confirmed their successful synthesis. Figure 3 shows the NMR spectra of deacetylated and butyl-modified chitosan on the top and bottom, respectively. The absence of peaks near 175 ppm and 20 ppm in the deacetylated chitosan spectrum, where the carbonyl and methyl carbons of the acyl group would be expected to appear, respectively, verified that the polymer was almost completely deacetylated.⁴ The signals present at 105, 84, 76, 75, 60, and 57 ppm are indicative of the carbohydrate backbone, assigned as carbons 1, 4, 3, 5, 6 and 2, respectively.⁴

The NMR spectrum obtained for the butyl-modified chitosan confirmed that a butyl chain was introduced on the polymer backbone via reductive amination by the appearance of signals at 51, 32, 21, and 14 ppm corresponding to the butyl carbons, starting with the carbon attached to the amine of the polymer and moving toward the carbon of the methyl group, respectively.⁴ The signals representing the backbone are shifted slightly to 104, 84, 75, 73, 63, and 61 ppm. The degree of butyl substitution on the chitosan polymer is roughly 1:1, as determined from the peak integrations (although it is known that carbon integrations are not very accurate due to long spin-lattice relaxation times and uneven signal enhancement by the nuclear Overhauser effect).

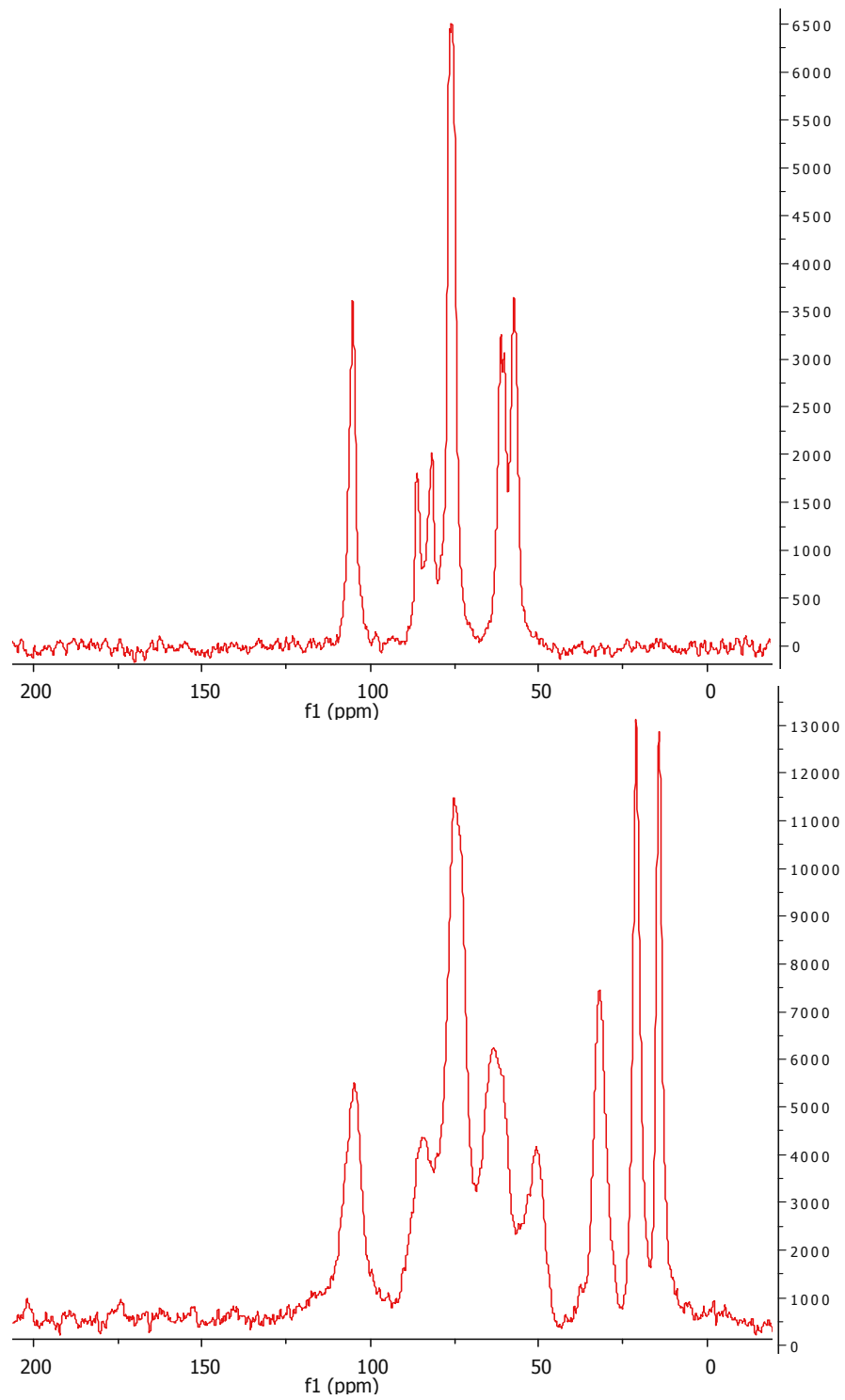


Figure 3. Solid-state ^{13}C NMR spectra of deacetylated (top) and butyl-modified chitosan (bottom).

Broadening of the peaks in the butyl-modified chitosan was observed, which could be indicative of much higher molecular weight analytes. In the present case, a possible explanation involves branching or cross-linking of the polymer due to ring opening and closing during the hydrophobic modification reaction. Despite these possible issues, the NMR spectra largely confirmed the successful synthesis and modification of the deacetylated and butyl-modified chitosan.

THE AIR-DRYING METHOD AND SUBSTRATE PROPERTIES

The method chosen for drying the films has potential to introduce variations in the film thicknesses that are not a direct result of the polymer's characteristics or the deposition method. For example, freeze drying is a technique known to produce chitosan scaffolds that are rather porous due to the growth of ice crystals upon freezing and their subsequent vacuum sublimation.⁴ However, relatively strong forces are involved in this process that would disrupt and alter the film thickness. In this case, the decreased density of water upon temperature-induced crystallization would increase the volume and thickness of the film. Therefore, the air-drying method was chosen to minimize the impact on the resultant films.

Correlations between deposition rates and film thickness of air-dried films should hold for the films immediately before they are air-dried (after they are deposited) and after they are air-dried. In other words, the only effect of air-drying on film thickness is assumed to reduce film height by a uniform factor across all films. This assumption is considered reasonable because the drying process is dominated by the evaporation of a solvent (acetic acid and water). Although the residual solvent content was not monitored,

it should be consistent among the films as they were all dried by the same procedure under a controlled humidity atmosphere via desiccation. As such, the evaporation process should be consistent across all films and introduce negligible shear forces. The exception to the uniformity of the evaporation process occurs near the edges of the film, making it imperative that these edge effects be detected, identified, and discarded from the analysis of the film thickness. After careful examination of the films, it was determined that approximately 0.5 – 1.0 cm was sufficiently distant from the edge to avoid the unpredictable regions of the film with respect to thickness.

It is also assumed that any effect of the support substrate (i.e., glass slide) surface on any correlation found should be consistent and negligible. This is considered reasonable because the films, although micron thin, are still orders of magnitude larger than the surface height of any molecular functional groups that may permeate the surface of the glass slide. Specifically, the hydroxyl groups on the surface of the substrate, arising from the pretreatment of the glass slides with piranha solution, are on the order of Ångstroms and are at least 100x smaller than the thickness of the films. A relevant consequence of having a hydroxylated surface is increased hydrophilicity, allowing the aqueous solution to be readily spread across the substrate. As such, the effect of any chemistry between the surface of the glass slide and the polymer solution is considered negligible relative to the fluid forces dominating the distribution of polymer solution during the deposition along the surface of the glass slide. Also, as the glass slides are uniformly manufactured and pretreated with piranha solution, the impact of surface chemistry with molecules in solution should also be consistent across all samples,

therefore canceling out of any relative comparison. For all of these reasons the thickness of all films, all other deposition conditions remaining constant, are reproducible.

IMPACT OF THE RAZOR BLADE INCISION ON FILM THICKNESS

In order to measure the film thickness, an incision in the film was made using a razor blade and the height difference between the film surface and the groove produced by the razor was taken to be the film thickness. To test the accuracy of the assumption that the method of making the incision in the film actually represents the surface of the glass and not a deeper groove produced by the impact of the razor blade, measurements were taken for a blank glass slide with no film deposited. Measurement of a blank microscope slide with slices similar to those made for the film thickness measurements yielded results ranging from 0.01 μm to 5.04 μm , as shown in Table 1, revealing an opportunity for personal systematic or gross error to cause inconsistencies in the data. Upon analysis, it was noted that the incision made by hand does indeed carve a groove into the glass substrate, whose depth is dependent on the amount of pressure applied to the cutting utensil. When a lot of pressure is applied by hand to the razor, deep grooves are inflicted on the glass substrate, varying greatly in depth, yielding unpredictable results that ranged anywhere from 0.18 μm to 5.04 μm . This is especially significant when compared to the expected magnitude of the films intended to be deposited ($\approx 0.1 \mu\text{m} - 0.2 \mu\text{m}$). Even when little pressure is applied by hand to the cutting implement, the substrate surface is still impacted, yet to a much lesser extent, about 0.01 μm . Preliminary analysis of films cut with the razor by hand showed that although a small amount of pressure does minimal damage to the surface of the blank glass slide, it is not enough to

completely cut through the chitosan film and reach the glass surface. As this problem would be present for any measurement technique, such as profilometry, a backup measurement would not suffice to address this inconsistency. Instead, to ensure that the incision was more uniform and deep enough to carve completely through the chitosan film, an apparatus was constructed that would provide a more consistent pressure during the cutting process by providing a constant weight on the razor blade.

Pressure	Depth (μm)
Light (Hand Made)	0.01
	0.02
	0.01
Heavy (Hand Made)	5.04
	2.56
	0.18
Uniform (Apparatus Made)	0.35
	0.32
	0.35
	0.29
	0.31

This apparatus was custom made with a plate attached to a stationary pivoting point and the razor attached at the end of the plate opposite from the pivoting point, allowing the pressure applied to the razor to be controlled by the user. This data is also presented in Table 1, showing that the pressure applied by the apparatus resulted in a more consistent depth of the incision, on average $0.32 \pm 0.03 \mu\text{m}$. The assembly of such a device solved the issue of applying a consistent pressure, however, it did not address

whether or not the measurements taken for the film thicknesses actually represent the substrate surface.

Although the amount of pressure applied to the cutting utensil greatly influences the depth of the resulting surface incision relative to the magnitude of the film thicknesses, this effect can be considered negligible for the chitosan films based on the measurement technique. More specifically, the width of an incision produced on a slide coated with a chitosan film is much larger than the incision on a blank slide and the blade of the razor, indicating that on the edge of the slice there is a region where the film is torn away from the glass slide. In other words, the width of the incision is increased by the tearing away of the chitosan film down to the surface of the microscope slide, seen in Figure 4 as a relatively smooth section. Although this torn section may be related to the rate or the angle at which the incision is made, these parameters were not tested as it is only necessary to obtain a torn section and not control the size, frequency, etc. The top left is the camera image (top-down view) of the film showing where the film was torn from the glass substrate during the incision process. The incision runs from the left to right across the image and just above the edge of the incision are the areas where the film was torn away from the substrate. The top right shows the topographical image of the film where different heights are represented in color (red being the highest and blue being the lowest). In this image, the green, yellow, orange, and red areas show where the torn parts of the film end while the blue regions show the surface of the film and the surface of the substrate. In both of the top images, the blue line on the left side represents the location of the cross section analyzed for the film thickness. The bottom image shows the cross section of the film used for the actual measurements, where the film height was

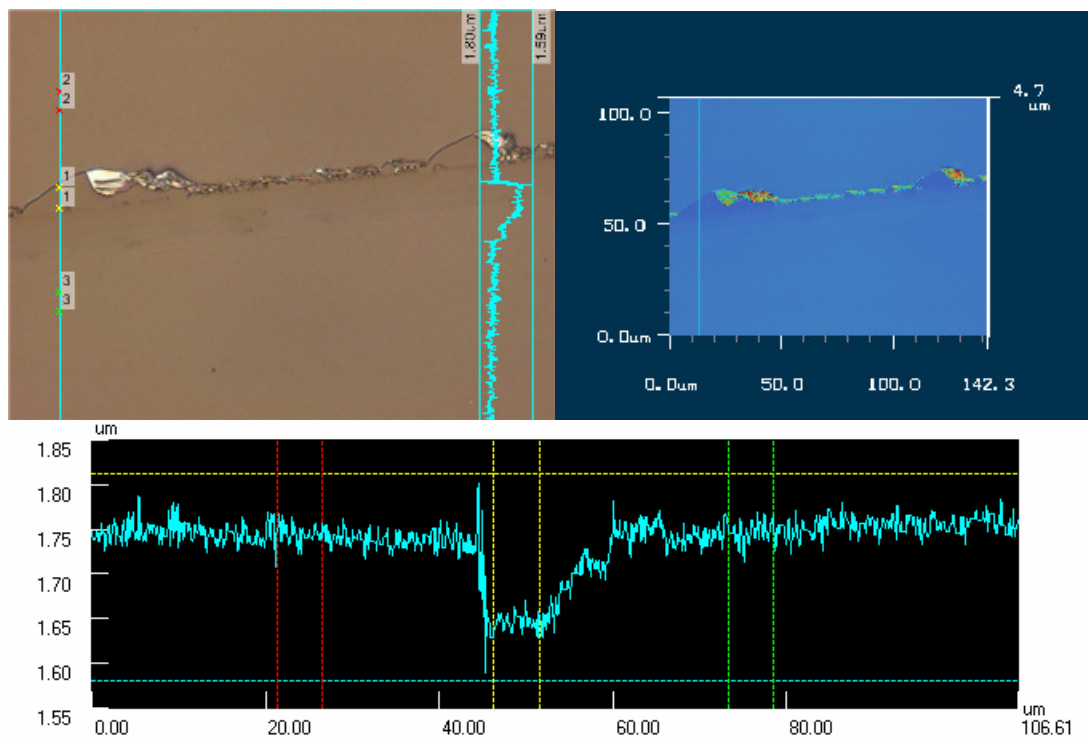


Figure 4. Images from the Keyence microscope for a film prepared from 2% (w/w) deacetylated chitosan in 0.5 M acetic acid at 17 cm/hr, exemplifying the measurement technique. The camera image is on the top left, the topographical image is on the top right, and the cross section of the film (across the incision) is on the bottom.

averaged over the sections between the dashed red and green vertical lines and the glass substrate height was averaged over the section between the dashed yellow vertical lines. The height difference between the film and the glass substrate was taken to be the film thickness. The smooth region, shown between the vertical dashed yellow lines in the cross section, is where a reasonable assumption was made (based on the reproducibility of the measurement and the smoothness of this region) that the surface of the glass was actually reached. Although this region was taken to be the surface of the glass slide, systematic error could arise if not all of the film was torn away due to strong interaction with the substrate surface. Instead of the deepest section of the incision, the smooth region, which is assumed to represent the glass surface, was used to measure the

thickness of the films. If this were not the case, one would expect the standard deviation to be unreasonably large, i.e., larger than the thickness. Upon realizing the inconsistencies in the depth of the incision in the glass, precautions were taken during the measurement of the film thickness, along with afore mentioned adjustments in the methodology.

REPRODUCIBILITY OF THE FILM THICKNESS AND THE MICROSCOPE

To determine the reproducibility of the microscope, images were taken and thickness measured for the same location of a blank slide 20x and the standard deviation was calculated from these measurements. The measured average depth of the incision was $0.08 \pm 0.01 \mu\text{m}$. These results, reported in Table 2, show that upon repeated measurement of the same image 20x, the precision of the instrument was found to be $0.01 \mu\text{m}$, as calculated from the standard deviation of the measurements. The limit of detection is three times the standard deviation, in this case equal to $0.03 \mu\text{m}$. The noise level of the instrument ($0.01 \mu\text{m}$) is on the same order of magnitude as the measurement itself, indicating that the thickness of the films ($0.08 \mu\text{m}$) is approaching the limit of the microscope's measurement ability. The magnitude of the noise level measured for the glass substrate and the film surface was on the micron scale, revealing that the microscope has inherent limitations in regards to its measurement capabilities on the order of magnitude desired in the present work. The magnitude of the noise should not have a large impact on the measurement of the film thicknesses, however, because the measured thicknesses are an average height difference over an area, thereby minimizing its effect.

Image #	Depth (μm)	Image #	Depth (μm)
1	0.08	12	0.09
2	0.08	13	0.08
3	0.08	14	0.07
4	0.08	15	0.07
5	0.08	16	0.08
6	0.08	17	0.08
7	0.07	18	0.09
8	0.08	19	0.07
9	0.08	20	0.08
10	0.08	Average	0.08
11	0.08	σ	0.01

To determine the reproducibility of film thickness with respect to deposition rate, two different deposition rates were chosen somewhat arbitrarily; one toward the lowest value of the possible syringe pump rates (2.0 cm/hr) and the other near the upper value (20.0 cm/hr). The chosen rates also needed to be within the range of rates that would produce controllable film thicknesses, although this limitation is inherently confirmed or refuted by the results, as they will not be reproducible if the chosen deposition rate is not within the proper range. Measurements recorded for 5 different deacetylated chitosan films made at deposition rate of 20.0 cm/hr are presented in Table 3. The average thickness and standard deviations calculated for films 1 – 5 together is $0.04 \pm 0.02 \mu\text{m}$, which is approaching the limit of detection ($0.03 \mu\text{m}$). Films numbered 1 – 5 individually range in average thickness from 0.02 to $0.06 \mu\text{m}$ with standard deviations ranging from 0.01 to $0.03 \mu\text{m}$. The relative standard deviations of the data are about 50% of the films' thickness which is on the same order of magnitude as the measurements. These are

relatively large standard deviations with respect to the film thicknesses, suggesting that the surface morphology of the films is not uniform on the level of the measurement.

Film #	Thickness (μm)	σ (μm)
1	0.04	0.02
2	0.03	0.01
3	0.02	0.01
4	0.06	0.03
5	0.03	0.01
Average	0.04	0.02

Table 4 presents data collected for 5 different deacetylated chitosan films produced at a deposition rate of 2.0 cm/hr. Overall, the average thickness and standard deviation for films numbered 1 – 5 is $0.14 \pm 0.07 \mu\text{m}$. The average thickness of the films made at the slower rate was larger, as predicted in the literature,²⁴ although a more in depth discussion of this relationship is presented later. The thickness of these films ranged from 0.11 to 0.18 μm with standard deviations ranging between 0.05 and 0.08 μm . The relative standard deviations are also close to 50%, implying that the morphology of the surface is not reproducible on the order of the micron scale.

Film #	Thickness (μm)	σ (μm)
1	0.13	0.08
2	0.18	0.05
3	0.12	0.06
4	0.15	0.07
5	0.11	0.05
Average	0.14	0.07

The standard deviations reported in Tables 3 and 4, presented graphically in Figure 5, neglect edge effects, which were found to be too unpredictable to include in the average thickness and relative standard deviation calculations. Therefore, data was not collected and reported for these regions, as mentioned previously. The greater standard deviations for the films made at 2.0 cm/hr indicate lower precision than those made at 20.0 cm/hr, suggesting that films produced at the slower deposition rate are not reproducible or that the surface morphology of all films was not uniform on the level of the microscope's measurements, with fluctuations in height across the film greatest at the lower deposition rate.

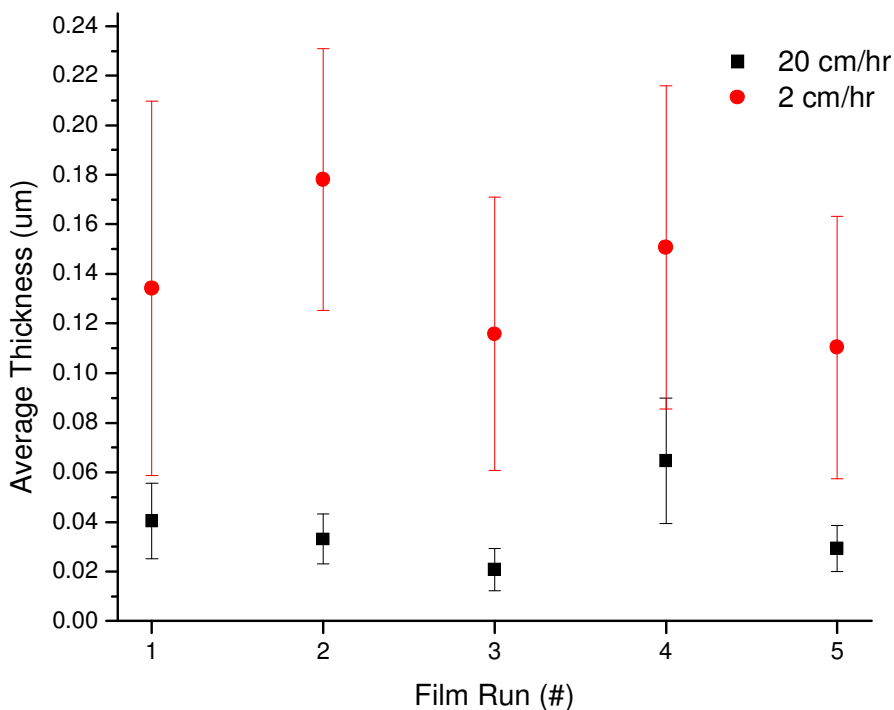


Figure 5. Reproducibility plot of film thickness vs. film # for 5 films prepared from 2% (w/w) deacetylated chitosan in 0.5 M acetic acid at both 2 and 20 cm/hr. Each set of films are represented in a different color: the set prepared at 2 cm/hr in red and the set prepared at 20 cm/hr in black.

It is important to note that these films were part of preliminary analyses, performed to determine if the experimental methods were valid. Until this point, the same solution of deacetylated chitosan was used over a period of time, approximately 2 months, to prepare all of the films from a batch of chitosan available in the laboratory. It was not until after preparation of a new batch of chitosan that a difference in color of the solution as well as a visually perceivable decrease in the viscosity of the solution over time was noticed. The difference in solution color and the sharp decrease in solution viscosity of the former batch were found to be attributed to sodium hydroxide not being completely washed from the chitosan upon removal from the autoclave. The new batch prepared was thoroughly washed until neutrality (tested with pH indicator strips) and solutions were freshly prepared for each set of experiments to avoid significant degradation of the chitosan polymer. These results, therefore, only validate the method chosen to measure the film thicknesses and not the actual values found. If this experiment were repeated using fresh solutions, it is possible that the results would be more precise.

CHAPTER 4:

FILM THICKNESS VS. DEPOSITION RATE OF SPREAD-COAT CHITOSAN FILMS

INTRODUCTION

In the hope that spread-coat micron thin chitosan films could become an alternative material for enzyme immobilization in engineering biofuel cells, the ability to predict and control the thickness of the films is imperative. This study aims to prepare chitosan films at various deposition rates using the spread-coating method, while keeping all other parameters constant in order to establish the relationship between film thickness and deposition rate. It was expected that the correlation between the film thickness of chitosan films and deposition rate would be similar to those found for other materials previously studied using the spread-coating technique.^{24,26,27} However, the results of this study varied greatly from those found in the literature and are reported hereafter.

DEACETYLATED CHITOSAN FILMS

To characterize the thickness of 2% (w/w) air-dried deacetylated chitosan films as a function of deposition rate, films were spread-coated at different rates and the average thickness plotted (Figure 6). Rates for deacetylated chitosan film deposition were initially chosen starting at 2 cm/hr and incrementally increase by 2 cm/hr up to 20 cm/hr. Figure 6 shows the average film thickness of the first set of films in green (Solution 1). A second set of films were then prepared at the same deposition rates to verify the first set of data, shown in red (Solution 2). A trend began to become apparent with the exceptions at the

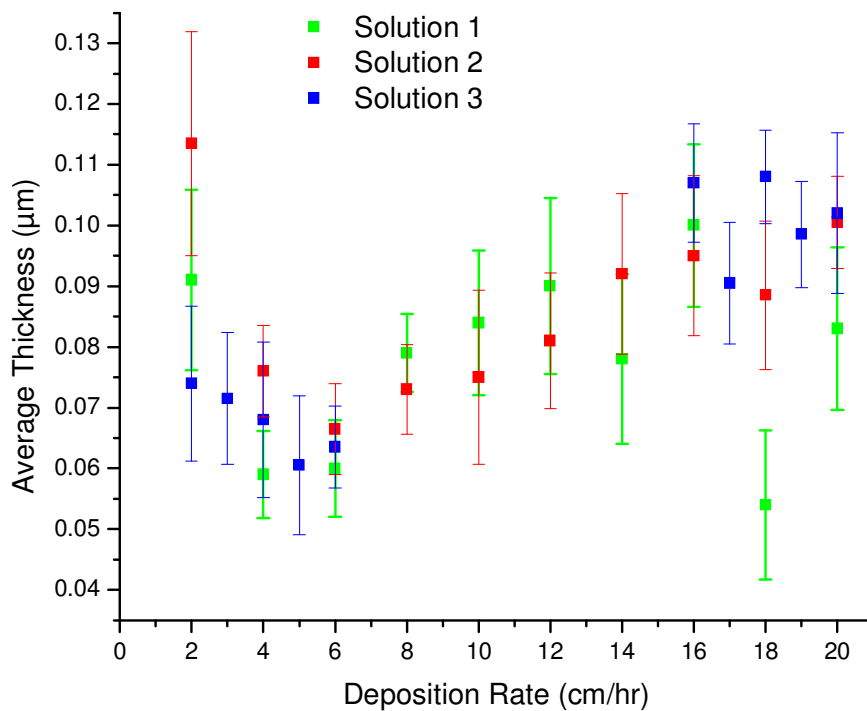


Figure 6. Plot of film thickness vs. deposition rate for films prepared from 2% (w/w) deacetylated chitosan in 0.5 M acetic acid. Each set of films are represented in a different color: the first set in green (Solution 1), the second set in red (Solution 2), and the third set in blue (Solution 3).

Solution 1			Solution 2			Solution 3		
Rate (cm/hr)	Thickness (μm)	σ (μm)	Rate (cm/hr)	Thickness (μm)	σ (μm)	Rate (cm/hr)	Thickness (μm)	σ (μm)
2	0.09	0.01	2	0.11	0.02	2	0.07	0.01
4	0.06	0.01	4	0.08	0.01	3	0.07	0.01
6	0.06	0.01	6	0.07	0.01	4	0.07	0.01
8	0.08	0.01	8	0.07	0.01	5	0.06	0.01
10	0.08	0.01	10	0.08	0.01	6	0.06	0.01
12	0.09	0.01	12	0.08	0.01	16	0.11	0.01
14	0.08	0.01	14	0.09	0.01	17	0.09	0.01
16	0.10	0.01	16	0.10	0.01	18	0.11	0.01
18	0.05	0.01	18	0.09	0.01	19	0.10	0.01
20	0.08	0.01	20	0.10	0.01	20	0.10	0.01

higher and lower deposition rates. To clarify the relationship in these regions, a third set of films were prepared in 1 cm/hr increments from 2 to 6 cm/hr and 16 to 20 cm/hr, shown in blue (Solution 3). The data for these films is presented in Table 5. The film prepared at 18 cm/hr in Solution 1 seems to be an outlier data point.

The data suggests three distinct trends with respect to deposition rate, as shown in Figure 7: (i) an initial decreasing (inverse relationship) slope as the deposition rate increased from 2 to 5 cm/hr in red, (ii) an increasing (linear relationship) slope as the deposition rate increased from 5 to 16 cm/hr in blue, and (iii) a leveling out (saturation) of film thickness for deposition rates above 16 cm/hr in green.

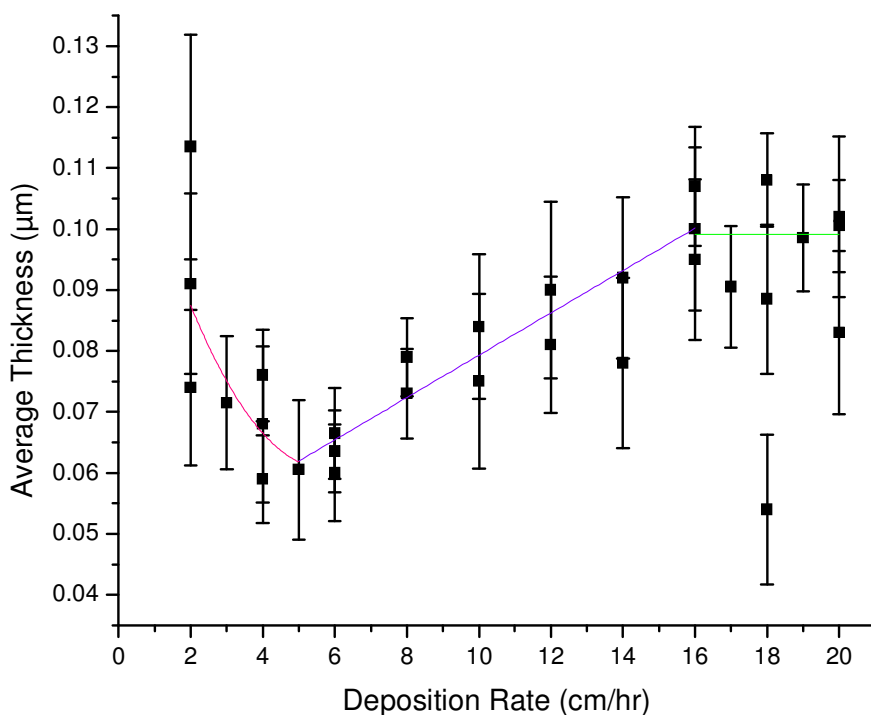


Figure 7. Plot of film thickness vs. deposition rate for films prepared from 2% (w/w) deacetylated chitosan in 0.5 M acetic acid, showing three regions of differing relationships: inverse decreasing in red, linear increasing in blue, and saturation (leveling out) in green.

Overall, film thicknesses ranged from 0.05 μm to 0.11 μm with standard deviations ranging from 0.01 μm to 0.02 μm , with a relative deviation of about 10% to 20%. These standard deviations are on the same order of magnitude as the measurement, implying that the morphology of the surface is not uniform on the order of the micron scale and that the measurement is approaching the instrument's limit, as discussed previously.

These results vary from those found in the literature for air-dried silica and ferritin films, which showed an inverse linear relationship between the deposition rate and film thickness across the full range of measured deposition rates.^{24,26} This result is reasonable due to the fundamental differences in chemical properties of the analyte and experimental parameters, such as solution viscosity and evaporation methods. In the system employed by Yuan et al. (2007) the structure of the film is formed through convective self-assembly of the molecules within the solution as the solvent (water) evaporates.²⁶ Convective self-assembly refers to the ordering of particles on a substrate under the guidance of convection forces that arise from the evaporation of a solvent, causing a flow of the particles toward the site of evaporation. In these systems, as the film deposition rate increases there is less time for solvent evaporation to induce convective self-assembly, an action that ultimately yields a thinner film. In the case of the chitosan system, the structure of the film is not controlled by convective self-assembly (evaporation takes place after film deposition instead of during), but rather is controlled by the character of intra- and intermolecular interactions between the polymer strands as well as the external forces that are exerted on the solution as the top slide is pushed forward.

The external forces that are imposed as the slide is pushed forward include (i) the downward force of gravity due to the mass of the upper slide (ii) a horizontal shear stress applied to the top of solution as the slide pushes forward, (iii) and a counter shear stress applied to the solution by the surface of the bottom stationary slide. As these forces are applied to the solution during deposition, the polymer chains must reorganize themselves in some manner that compensates for the applied forces.

The polymer's structural response to these external forces is largely governed by two time factors that involve the solution's intrinsic ability to reorient its polymer chains in response to the rate at which the upper slide move forward. Both of these motions (the polymer's response and the rate of deposition) possess time factors that may or may not be on the same order of magnitude. The rate of deposition is a known time factor from the experimental method, while the polymer's ability to change its structural orientation, based on the properties of the solution such as viscosity and other experimental parameters (including the strength of inter- and intramolecular interactions, solution concentration, etc.), is unknown and can only be loosely determined relative to the rate of deposition. The time factor involved in the polymer's structural response refers to the amount of movement of the molecules with respect to time. At slower deposition rates, for example the region between 2 and 5 cm/hr, the film thickness decreases with increasing deposition rate, i.e., it has a negative slope until reaching a minimum thickness. In this region, the polymer's time factor is greater than the rate at which the upper slide applies force. As such, the underlying molecular structure has enough time to reorient itself in response to the applied force and, as expected, the solution is spread thinner at higher deposition rates. This reorientation involves the polymeric backbone

folding (or unfolding) differently in order to compensate for the force of the upper slide. At a deposition rate of 5 cm/hr, however, a minimum is reached wherein the film thickness begins a transition to increase with increasing deposition rate until reaching a saturation point at 16 cm/hr. Within this region, the solution's time factor and the deposition rate are relatively equivalent, and the underlying molecular structure is increasingly unable to respond at the same rate as the applied force, resulting in the solution acting more like a solid and beginning to push the top slide upward. The result is that the film thickness begins to increase linearly with deposition rate until the polymer's time factor begins to become smaller than the rate at which the top slide applies forward force. At this point the solution has exerted as much upward force against the slide as possible, and no further increase in the deposition rate will yield a higher film thickness.

BUTYL-MODIFIED CHITOSAN FILMS

To characterize the thickness of 2% (w/w) air-dried butyl-modified chitosan films as a function of deposition rate, films were prepared as described above and the average thicknesses were compared to the deposition rates. Deposition rates were chosen by starting at 2 cm/hr and incrementally increasing by 2 cm/hr up to 20 cm/hr, as was done for deacetylated chitosan. Figure 8 shows the average film thickness of the first set of films in green (Solution 1). A second set of films were then prepared to clarify the lower region of deposition rates (2 to 5 cm/hr) and to determine where saturation occurs in the region of higher deposition rates (25 to 40 cm/hr), shown in red (Solution 2). At this point, the trend became noticeable but more clarification of the higher and lower regions was necessary. To further clarify the relationship in these regions, a third set of films

were prepared incrementally from 3.5 to 5.5 cm/hr and from 20 to 26 cm/hr, shown in blue (Solution 3).

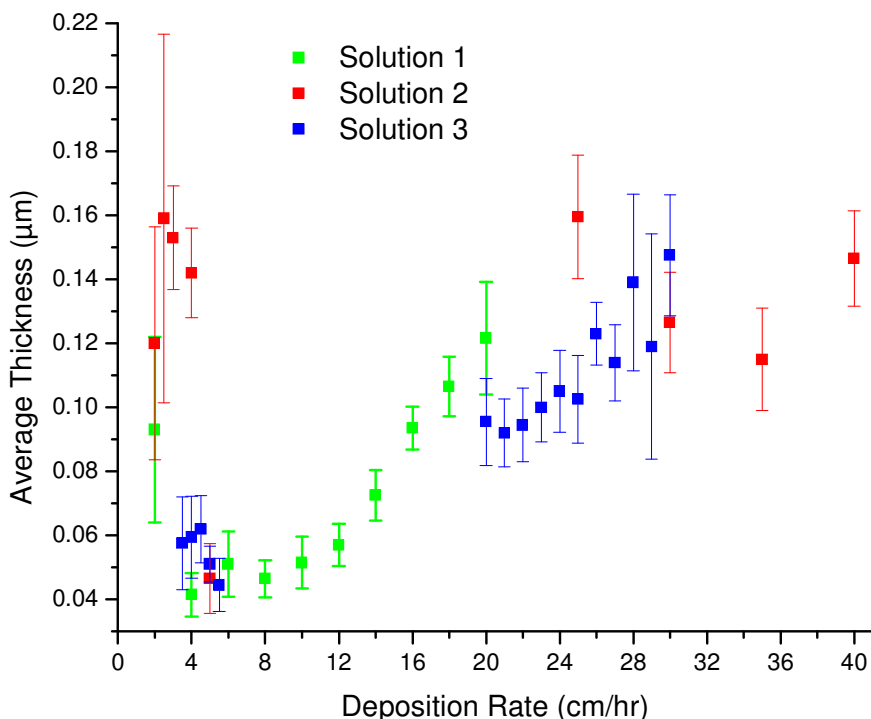


Figure 8. Plot of film thickness vs. deposition rate for films prepared from 2% (w/w) butyl-modified chitosan in 0.5 M acetic acid. Each set of films are represented in a different color: the first set in green (Solution 1), the second set in red (Solution 2), and the third set in blue (Solution 3).

The data for these films is shown in Table 6. Butyl-modified chitosan displayed a similar trend, shown in Figure 9, to that demonstrated by the deacetylated chitosan. Specifically, the same three major regions were observed; however, the regions were extended to yield a much broader range wherein the deposition rate and solution's internal time factor were relatively equivalent. That said, the initial transition point remained similar, 6 cm/hr, although the saturation deposition rate was increased from 16 cm/hr (for the deacetylated chitosan) to 30 cm/hr (for the butyl-modified chitosan). Film thicknesses ranged from 0.04 µm to 0.16 µm with standard deviations of ranging from

0.01 μm up to 0.06 μm . These standard deviations are larger relative to the film thickness than that of the deacetylated chitosan, about 7% to 38%, suggesting that the hydrophobically modified chitosan possesses less uniform surface morphology.

Table 6. Deposition Rate vs. Film Thickness of 2% (w/w) Butyl-Modified Chitosan								
Solution 1			Solution 2			Solution 3		
Rate (cm/hr)	Thickness (μm)	σ (μm)	Rate (cm/hr)	Thickness (μm)	σ (μm)	Rate (cm/hr)	Thickness (μm)	σ (μm)
2	0.09	0.03	2	0.12	0.04	3.5	0.06	0.01
4	0.04	0.01	2.5	0.16	0.06	4	0.06	0.01
6	0.05	0.01	3	0.15	0.02	4.5	0.06	0.01
8	0.05	0.01	4	0.14	0.01	5	0.05	0.01
10	0.05	0.01	5	0.05	0.01	5.5	0.04	0.01
12	0.06	0.01	25	0.16	0.02	20	0.10	0.01
14	0.07	0.01	30	0.13	0.02	21	0.09	0.01
16	0.09	0.01	35	0.12	0.02	22	0.09	0.01
18	0.11	0.01	40	0.15	0.01	23	0.10	0.01
20	0.12	0.02	-	-	-	24	0.11	0.01
-	-	-	-	-	-	25	0.10	0.01
-	-	-	-	-	-	26	0.12	0.01
-	-	-	-	-	-	27	0.11	0.01
-	-	-	-	-	-	28	0.14	0.03
-	-	-	-	-	-	29	0.12	0.04
-	-	-	-	-	-	30	0.15	0.02

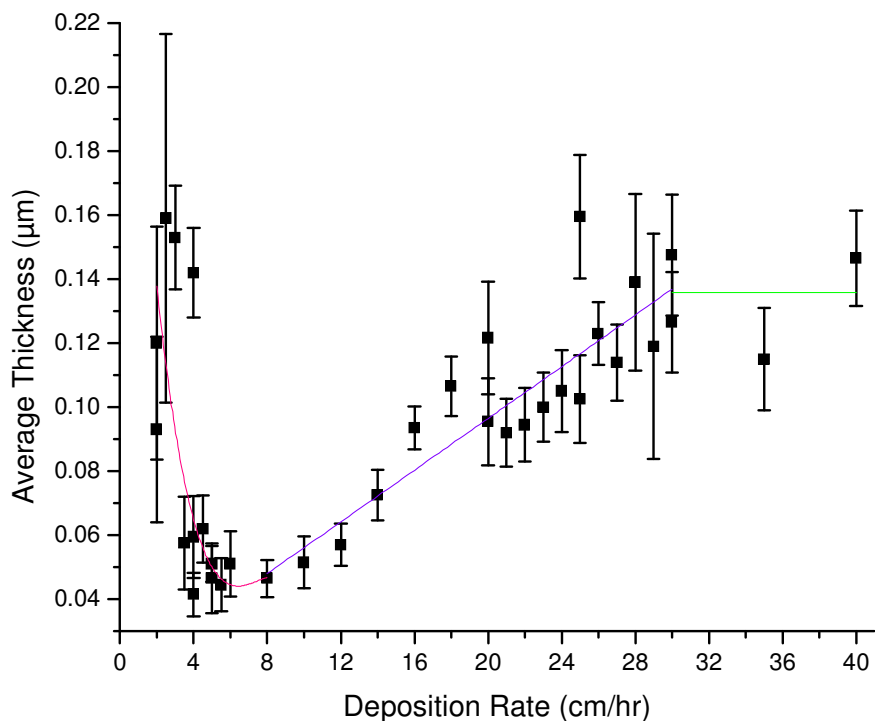


Figure 9. Plot of film thickness vs. deposition rate for films prepared from 2% (w/w) butyl-modified chitosan in 0.5 M acetic acid, showing three regions of differing relationships: inverse decreasing in red, linear increasing in blue, and saturation (leveling out) in green.

The key difference between the deacetylated and butyl-modified chitosan solutions lies in the hydrophobic modification of the polymer, which ultimately modifies the underlying state of aggregation and micellar structure (i.e., the relative degree of intra- vs. intermolecular interaction). Deacetylated chitosan, as prepared according to the procedures, is approximately 95% deacetylated, indicating that there are very few hydrophobic moieties remaining on the otherwise hydrophilic polymer backbone. This situation suggests that there is very little hydrophobic aggregation within a polymer strand or between polymer strands. Therefore, based on the solution concentration of the polymer, it is expected that the deacetylated chitosan polymer would promote more intermolecular interactions (relative to the butyl-modified chitosan), leading to a more

uniform surface morphology with smaller standard deviations for film thickness. The hydrophobic modification of chitosan introduces a large amount of butyl chains in close proximity to each other. Due to the abundance of butyl chains, it is likely that the hydrophilic and hydrophobic regions of the modified chitosan polymer promote intramolecular aggregation and, therefore, have more distinctly hydrophilic and hydrophobic domains in solution that upon evaporative drying leave the surface morphology less uniform, on the order of 0.01 to 0.06 μm , as is suggested by the standard deviations.

These differences also impact the capacity of the underlying polymer molecular structure to adapt and reorganize in response to an external shear stress. The stronger the inter- and intramolecular forces, the less the polymer will be able to adapt its molecular structure when an external force is applied, which would cause the moving upper slide to be forced up and over the solution rather than through it (spreading). While the same external shear forces were applied to both polymers, the hydrophobically modified polymer displayed stronger intramolecular forces that yielded an increased resistance to spreading and therefore have a thicker layer of solution left behind in the meniscus (Figure 2) that is formed behind the upper slide. This added aspect permits the butyl-modified polymer to better resist the action of spreading compared to that of the deacetylated polymer, therefore, yielding thicker films at a given deposition rate.

CHAPTER 5:

SOLUTION MICELLAR CHARACTERISTICS VIA VISCOSITY AND FLUORESCENCE

INTRODUCTION

It is essential to determine how hydrophobic modification affects the micellar structure of chitosan solutions in order to better understand how the modification affects the morphology of the resultant thin films prepared. To confirm the varied micellar structure of solutions of deacetylated and butyl-modified chitosan polymer, the viscosity of each solution was correlated to concentrations ranging between 0% to 3% (w/w) in complement with fluorescence spectroscopy, using 1-pyrenebutanoic acid as a hydrophobic probe.

VISCOSITY OF CHITOSAN SOLUTIONS

The relationship of viscosity to solution concentration was found to be predominantly dictated by the amount (relative dominance) and type of interactions (intra- or intermolecular) that occurred between the hydrophobic domains of the deacetylated or butyl-modified chitosan polymer. Although intra- and intermolecular interactions are present for all solution concentrations, the relationship between viscosity and chitosan concentration differed for the deacetylated and butyl-modified polymers due to variation in the relative dominance of these interactions. The solution viscosity was plotted against the polymer concentration to elucidate which of the two forces were relatively more dominant. The viscosity measurements, shown graphically in Figure 10

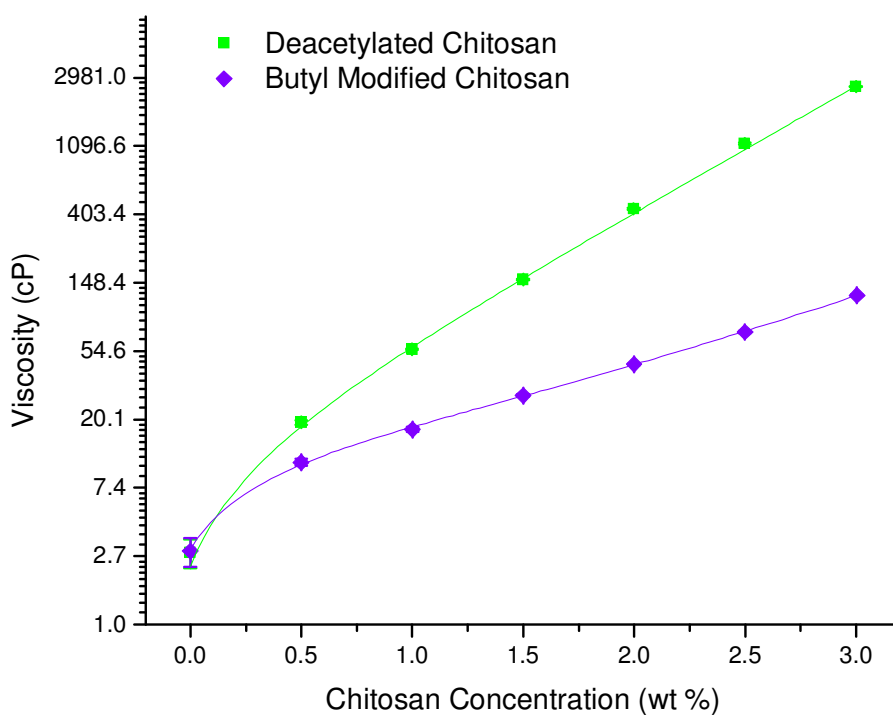
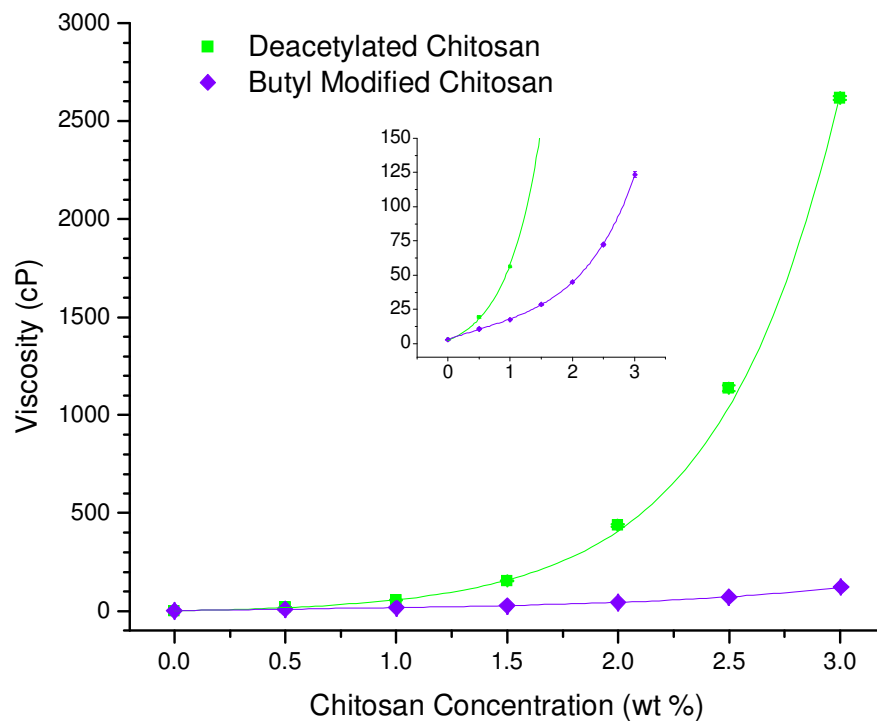


Figure 10. Viscosity vs. chitosan concentration of deacetylated chitosan (green) and butyl-modified chitosan (purple) solutions in 0.5 M acetic acid. Inlayed plot shows enlargement of butyl-modified chitosan (top). Viscosity (on a logarithmic scale) vs. chitosan concentration of deacetylated and butyl-modified chitosan solutions in 0.5 M acetic acid (bottom).

with the data included in Table 7, confirmed that the deacetylated chitosan solutions (in green) possess more intermolecular interactions than that of the butyl-modified chitosan (in purple), which has more intramolecularly aggregated hydrophobic regions, as seen in the sharper exponential increase in viscosity with respect to polymer concentration for deacetylated chitosan. This is considered reasonable because more interaction between neighboring polymer chains will increase (relative to intramolecular interactions) the resistance of the solution to flow (or reorient) in the face of external forces. As such, only at relatively high concentrations does the butyl-modified chitosan solution begin to show a sharper increase in viscosity due to an increase of intermolecular interaction.

Deacetylated Chitosan			Butyl-Modified Chitosan		
Concentration (% (w/w))	Viscosity (cP)	σ (cP)	Concentration (% (w/w))	Viscosity (cP)	σ (cP)
3.00	2617	52	3.00	123.4	0.8
2.50	1137	9	2.50	72.3	0.2
2.00	438.3	5.2	2.00	45.11	0.12
1.50	155.4	2.1	1.50	28.58	0.13
1.00	56.05	0.50	1.00	17.41	0.17
0.50	19.30	0.07	0.50	10.77	0.07
0.00	2.88	0.06	0.00	2.94	0.12

The convergence of the deacetylated and the butyl-modified at low concentrations suggests that at these low concentrations, intramolecular interactions are dominant for both deacetylated and butyl-modified chitosan. This explanation is reasonable because at low concentrations the occurrence of different polymer strands in close enough proximity to have an intermolecular interaction is less common, while the polymer is still able to fold on itself and interact intramolecularly. Although both deacetylated and butyl-modified chitosan show an exponential increase in viscosity with respect to increasing

concentration, the effect is much more pronounced for that of the deacetylated chitosan solutions. As the concentration increases, the frequency of collisions between neighboring polymer strands increases as well as their proximity to one another and therefore, the number of intermolecular interactions also increases. For deacetylated chitosan possessing relatively little amphiphilic nature, this suggests that the solution micellar structure is highly interconnected, causing the solution to become more resistant to flow due to a larger number of intermolecular interactions. However, for butyl-modified chitosan, the hydrophobic side chains induce amphiphilicity and promote the aggregation of the side chains within a polymer strand, i.e., more intramolecular interactions. An increased preference to aggregate contributes to intramolecular forces dominating at much higher concentrations than that of the deacetylated chitosan, therefore, the strength of the solution to resist deformation does not increase as rapidly.

The literature reports the opposite trend for the viscosity than what was observed in this set of experiments; the exponential increase in viscosity with respect to increasing chitosan concentration was sharper for the hydrophobically modified chitosan than that of the deacetylated.²⁰ A few factors account for the discrepancies with the literature including the degree of deacetylation, the degree of substitution, and the length of the side chain. Specifically, the deacetylated chitosan prepared in this work is more thoroughly deacetylated and the butyl-modified chitosan has a higher degree of hydrophobic substitution, about 95% with a 4 carbon alkyl chain, compared to 88% deacetylated and only 4% substituted with a 12 carbon alkyl chain.²⁰ According to Jiang et al., 2006, increasing the length of the alkyl chain and decreasing the degree of deacetylation both contribute to the onset of aggregation at lower concentrations, as

determined by fluorescence spectroscopy with pyrene as the probe.³ Therefore, it seems reasonable that the viscosity of hydrophobically modified chitosan with a 12 carbon alkyl chain increases more rapidly at lower concentrations than the native chitosan. Moreover, with a lower degree of hydrophobic substitution, intramolecular aggregation is less likely for a polymer with such a high degree of ionization²⁰ (based on the proximity of other alkyl chains), and the viscosity would increase much more rapidly with the concentration than the deacetylated chitosan.

FLUORESCENCE SPECTROSCOPY OF CHITOSAN SOLUTIONS

To confirm the presence of hydrophobic domains in deacetylated and butyl-modified chitosan, fluorescence spectroscopy was performed using 1-pyrenebutanoic acid as a probe, using an excitation wavelength of 338 nm. Fluorescence spectra were first acquired for solution concentrations matching that of the viscosity experiments. However, to clarify the relationship in the lower region of chitosan concentrations it was necessary to prepare and analyze much more dilute solutions (including an overlapping data point so that the two sets of experiments could be compared). Data obtained for the fluorescence emission spectra is plotted in Figures 11 and 12. The emission spectra of the deacetylated chitosan solutions of low concentration are shown on the top of Figure 11, while those of the higher concentrations are on the bottom. Each solution is shown in a different color. Likewise, Figure 12 contains the emission spectra of butyl-modified chitosan solutions of low concentrations on the top and high concentration on the bottom, each in a different color.

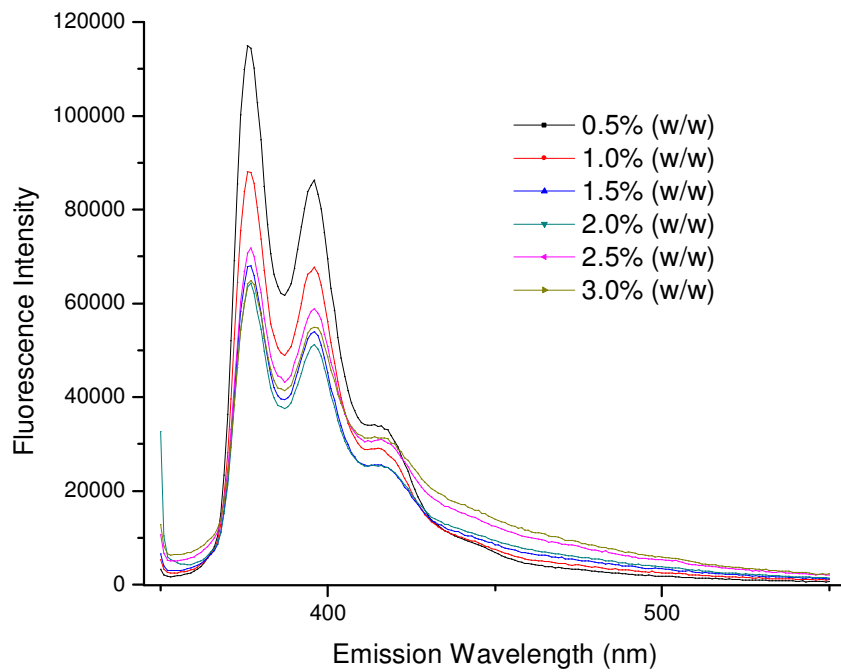
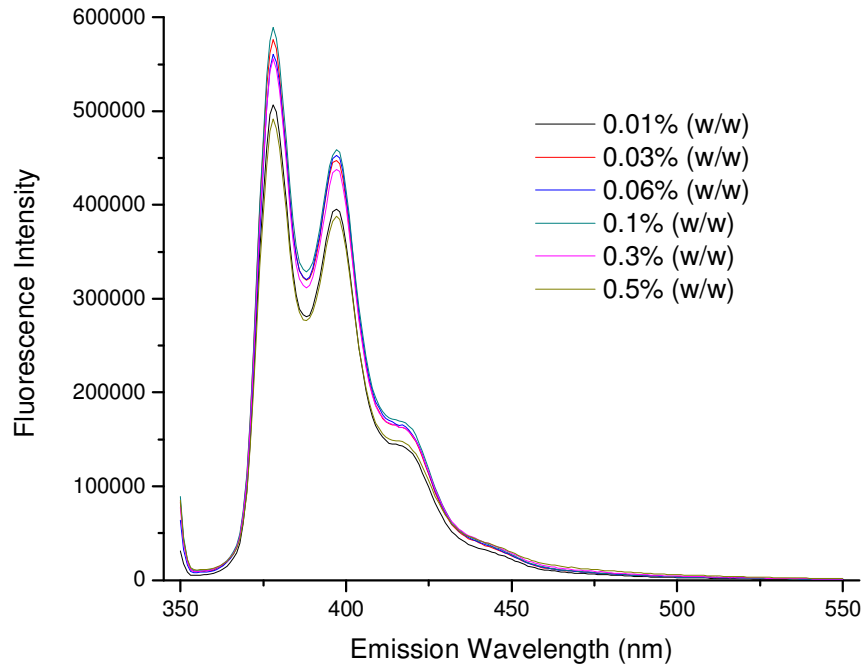


Figure 11. Fluorescence emission spectra of deacetylated chitosan (low concentrations on the top and high concentrations on the bottom).

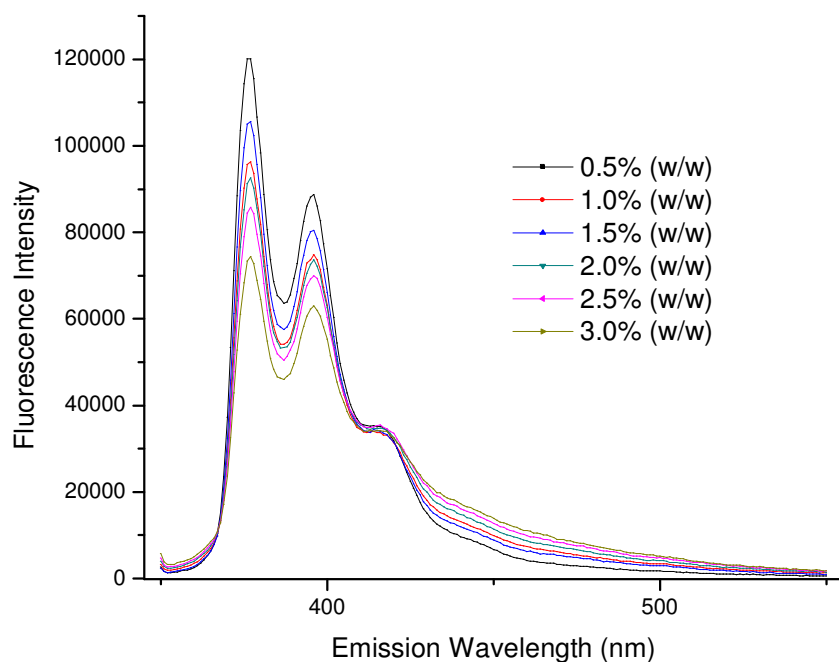
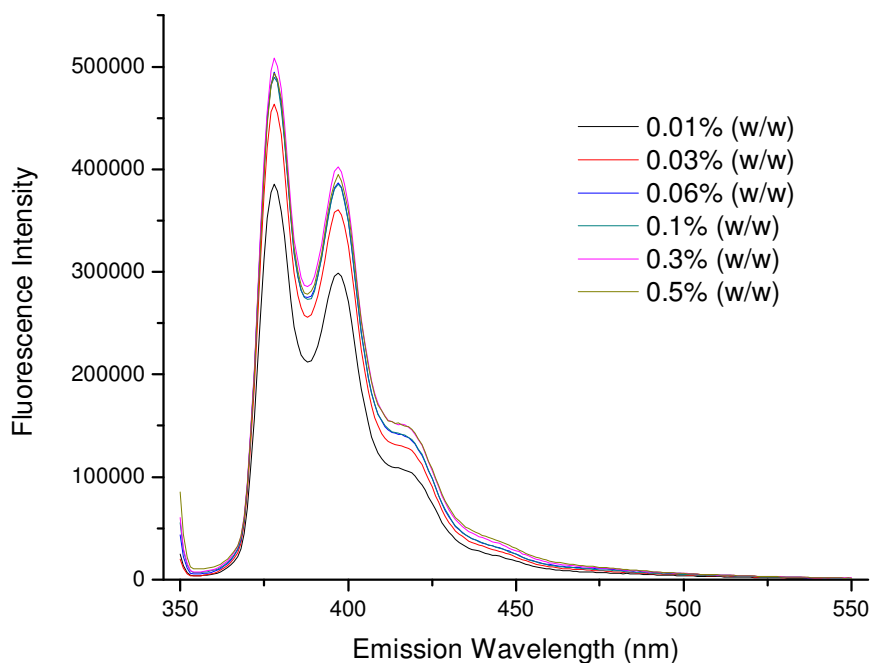


Figure 12. Fluorescence emission spectra of butyl-modified chitosan (low concentrations on the top and high concentrations on the bottom).

Although it is difficult to determine visually from Figures 11 and 12, Table 8 reports the ratio of the maximum intensities of the first and third vibronic bands. These calculated ratios were found to be in accordance with the previous findings, showing an

observable decrease in the ratio of the first and third vibronic energy bands (in the emission spectra of 1-pyrenebutanoic acid) in the presence of both deacetylated and butyl-modified chitosan solutions with respect to an increase in concentration. The data for the ratio of the first and third vibronic bands, shown graphically in Figure 13, confirmed that the intensity of the first peak of the fluorescence emission of 1-pyrenebutanoic acid decreased in deacetylated and butyl-modified chitosan, i.e., the ratio of the maximum peak intensities I_1/I_3 decreased in a less polar chemical microenvironment, suggesting the presence of hydrophobic domains in both chitosan species.

Deacetylated Chitosan		Butyl-Modified Chitosan	
Concentration (% (w/w))	I_1/I_3	Concentration (% (w/w))	I_1/I_3
0.01	3.50	0.01	3.54
0.03	3.48	0.03	3.54
0.06	3.38	0.06	3.50
0.10	3.45	0.10	3.44
0.30	3.37	0.30	3.35
0.50	3.31	0.50	3.24
0.50	3.37	0.50	3.39
1.00	3.04	1.00	3.07
1.50	2.67	1.52	2.83
2.00	2.52	2.01	2.66
2.50	2.32	2.50	2.42
3.00	2.06	3.00	2.17

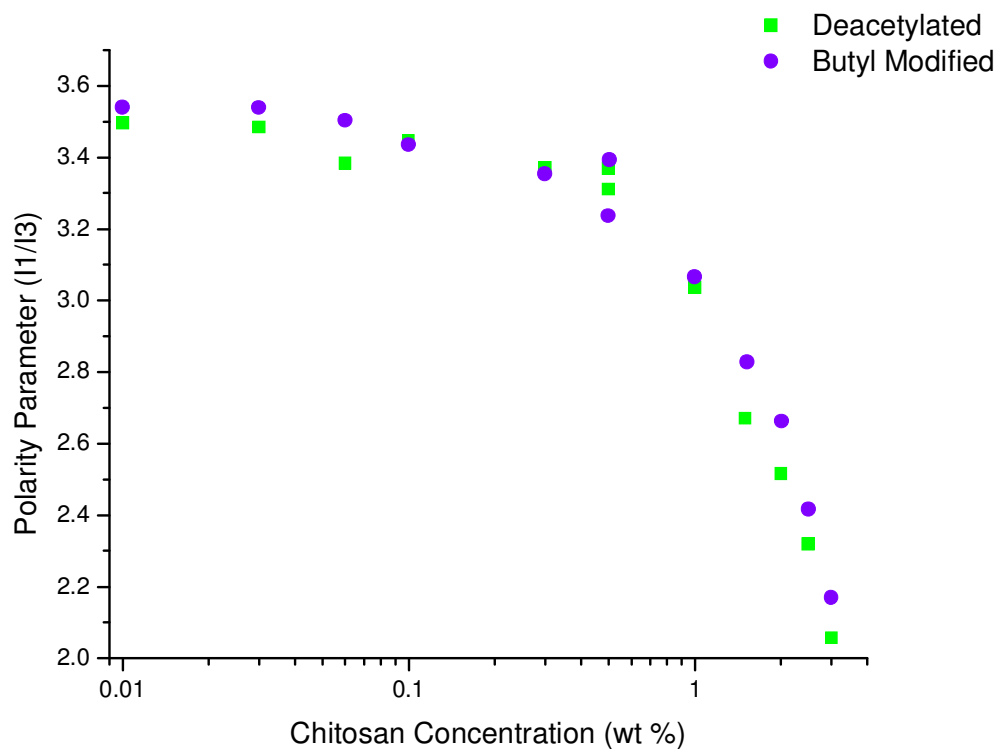


Figure 13. Plot of the polarity parameter (I_1/I_3) vs. chitosan concentration for deacetylated and butyl-modified chitosan solutions in 0.5 M acetic acid using 1-pyrenebutanoic acid as the probe.

Although the solution concentrations of both chitosan solutions showed a similar relationship to the polarity parameter, they incorporated the probe into a different type of hydrophobic domain.²⁰ Deacetylated chitosan possesses hydrophobic domains that result from the aggregation of the polymer in a highly interconnected manner. This means that the fluorophore is likely wedged near the connection points of the polymer strands, creating a nonpolar microenvironment. One possible explanation is that the fluorophore is sandwiched between the polymer strands due to the hydrophobicity of the top and bottom surfaces of the sugar. This is due to the orientation of the hydroxyl groups on the polymer, which are all equatorial, leaving the area above and below the ring hydrophobic.

Aggregation of these hydrophobic regions would allow for incorporation of the fluorophore.

Another thing to keep in mind is the degree of deacetylation. At first glance, it seems unreasonable to consider deacetylated chitosan as having hydrophobic domains of any type, as the deacetylation reaction removes hydrophobic acyl functional groups. However, this reaction leaves the polymer 95% deacetylated, indicating that of the approximate 1100 to 1900 monomers per polymer strand, there are about 50 to 100 monomers left per polymer strand that still contain an acyl group (based on the percent deacetylation and the average molecular weights of the polymer and of a monomer). At very low solution concentrations of the polymer, this amount may be negligible in regards to its effect on the micellar structure, but as the concentration is increased, so does the amount of acyl moieties causing them to become increasingly important as they can create hydrophobic domains in the solution. Due to the small size of the acyl groups, they would not likely contribute profusely to intramolecular aggregation in deacetylated chitosan; rather they could more efficiently act as intermolecular links between polymer strands. Furthermore, these acyl groups are still present through the reductive amination reaction, adding to the hydrophobicity of butyl-modified chitosan. However, because acetyl groups are not considered to be very hydrophobic, it is more likely that the hydrophobic domains observed in the fluorescence experiments are due to sandwiching of the polymer strands. As stated earlier, polysaccharides are known to be hydrophobic and although in this case the chitosan backbone is protonated, allowing it to be more water soluble, it would still have a preference to interact with another polymer strand rather than water molecules.

Butyl-modified chitosan also has hydrophobic domains that are a result of the hydrophobic moieties incorporating the fluorophore, resulting in a nonpolar chemical microenvironment. However, the origin of these hydrophobic domains is due mostly to the aggregation of the butyl side chains with a larger amount of intramolecular interactions than that of the deacetylated chitosan, consistent with the viscosity measurements.

According to the literature, the fluorescence emissions should be distinctly different for the deacetylated and hydrophobically modified chitosan, though both should show a decrease in the polarity parameter with increasing chitosan concentration.²⁰ As stated before, the nonpolar chemical microenvironments found in deacetylated chitosan solutions are likely created by the intermolecular aggregation, via sandwiching of the polymer strands. Due to the low concentration of the fluorophore (0.8 μM) along with the intermolecular aggregation of polymer strands, it is possible that an observable decrease in the intensity ratio I_1/I_3 occurs for deacetylated chitosan solutions. Alternatively, this may indicate that the butyl groups do not add an appreciable amount of hydrophobicity to the polymer. Although this is not supported by the viscosity experiments, in which the deacetylated and butyl-modified chitosan solutions showed distinctly different results, suggesting there is a difference in the aggregation models. In summary, the deviations from the results reported in the literature were attributed to the variations in the preparation of the chitosan polymer solutions.

CHAPTER 6:

CONCLUSIONS AND FUTURE DIRECTIONS

CONSLUSIONS AND SUMMARY

The thickness of spread-coated films made from both deacetylated and butyl-modified chitosan was correlated to deposition rate and solution micellar structure, demonstrating how differences in the underlying aggregate structure can, to a certain degree, impact the final film thickness. At intermediate deposition rates, the thickness of chitosan films was predictable with an increasing linear relationship and well controlled. Outside of this range of deposition rates, the thickness of the resultant films was found to be less controllable with a nonlinear relationship. Furthermore, it was shown that hydrophobic modification of the chitosan extended the range of deposition rates (from 5 – 16 cm/hr to 6 – 30 cm/hr) over which a linear relationship between film thickness and deposition rate were found. Hydrophobic modification also extended the range of thickness achieved, from 0.06 – 0.10 μm to 0.04 – 0.14 μm , although, with an increase in the standard deviations. The larger standard deviation indicates that the film morphology is less uniform on the order of magnitude of the measurement of the film thickness. These features are accredited to the domination of intramolecular forces at lower concentrations of hydrophobically modified chitosan solutions compared to equal concentration of the deacetylated chitosan solutions, as supported by the viscosity and fluorescence experiments. With more intramolecular aggregates, as in the hydrophobically modified chitosan, the film is expected to have regions that are varied in thickness to a greater extent than that of the deacetylated chitosan, which is dominated by intermolecular

polymer interactions. Although both deacetylated and butyl-modified chitosan solutions were found to have inter- and intramolecular interactions and hydrophobic domains able to incorporate a fluorophore, deacetylated chitosan is much more interconnected via intermolecular interactions at higher concentrations.

This work characterizes the relative micellar structure of deacetylated and hydrophobically modified chitosan polymers to the method of spread-coating to form polymeric films with controlled thickness. Viscosity experiments in complement with fluorescence measurements, using a hydrophobic fluorophore, suggest that deacetylated chitosan solutions have a much more interconnected structure with distinct hydrophobic domains, whereas butyl-modified chitosan solutions show distinct hydrophobic regions that are less interconnected, also capable of incorporating a hydrophobic fluorophore. This variation, based on hydrophobic modification, is important from the perspective that enzyme immobilization is likely to occur in hydrophobic regions of the encompassing polymer due to the nonpolar nature of the enzyme exterior in aqueous environments. Therefore, if the hydrophobic modification of chitosan polymer shows a higher affinity for a hydrophobic molecule, it is a possible candidate for the immobilization of an enzyme via encapsulation, although this observation is not confirmation that this will occur, rather it is only an indication of the increased likelihood of enzyme encapsulation being a result of the modification. The solution based micellar structure may be important in aiding the immobilization process; however, the enzyme is more likely to become fully immobilized during the drying process via entrapment, which indicates the necessity to examine further the deposition process of the polymeric film that will house the enzyme. This work also encompassed the investigation of the deposition of polymeric films via

the spread-coating method, but the immobilization of the enzyme within these films remains unexplored. Investigation into enzyme immobilization with respect to chitosan polymer films in comparison with other immobilization materials, such as Nafion polymer, would provide insight into the commercial applicability of chitosan as an immobilization polymer.

FUTURE DIRECTIONS

Although these experiments were carried out with the utmost due diligence, there is still room for improvement. For instance, the measurement of film thickness on the laser scanning microscope had advantages and disadvantages. An advantage of using the microscope was that it was noninvasive, while providing a measure of the film thickness along with an image of the film. Although the microscope itself was not invasive, cutting the slide with a razor blade had an adverse effect. The razor blade caused the film to be compressed and torn. It also cut into the glass slide creating difficulties in finding the surface of the substrate. A simple solution to this would be to use a thinner bladed instrument, or to utilize a noninvasive measurement technique. Another drawback of the current technique is that the measurements were approaching the limit of detection for the instrument. A second technique such as atomic force microscopy or profilometry would be invaluable in corroborating these results.

There are other complimentary studies that could also further the understanding and knowledge base regarding the micellar structure of chitosan polymer, such as light scattering experiments performed on the chitosan solutions. Also, different fluorophores could be used to investigate the hydrophobic domains of the deacetylated and butyl-

modified chitosan solutions to better determine their respective inter- and intramolecular interactions.

Repetition of the experiments in this study with Nafion polymer would provide comparison to an established enzyme immobilization material. In addition, it would also ascertain data on spread-coated Nafion thin films. Logically, the next step is to apply the spread-coating method to actual enzyme incorporation into the chitosan/Nafion thin films. Ultimately, the enzyme-immobilized thin films should be applied and tested in an enzyme catalyzed biofuel cell.

REFERENCES

- (1) Cooney, M. J.; Lau, C.; Windmeisser, M.; Liaw, B. Y.; Klotzbach, T.; Minteer, S. D. *Journal of Materials Chemistry* **2008**, *18*, 667-674.
- (2) Lau, C.; Cooney, M. J.; Atanassov, P. *Langmuir* **2008**, *24*, 7004-7010.
- (3) Jiang, G.-B.; Quan, D.; Liao, K.; Wang, H. *Carbohydrate Polymers* **2006**, *66*, 514-520.
- (4) Cooney, M. J.; Petermann, J.; Lau, C.; Minteer, S. D. *Carbohydrate Polymers* **2009**, *75*, 428-435.
- (5) Klotzbach, T. L.; Watt, M.; Ansari, Y.; Minteer, S. D. *Journal of Membrane Science* **2006**, *282*, 276-283.
- (6) Klotzbach, T. L.; Watt, M.; Ansari, Y.; Minteer, S. D. *Journal of Membrane Science* **2008**, *311*, 81-88.
- (7) Martin, G. L.; Minteer, S. D.; Cooney, M. J. *ACS Applied Materials & Interfaces* **2009**, *1*, 367-372.
- (8) Martin, G. L.; Ross, J. A.; Minteer, S. D.; Jameson, D. M.; Cooney, M. J. *Carbohydrate Polymers* **2009**, *77*, 695-702.
- (9) Sjolholm, K. H.; Cooney, M.; Minteer, S. D. *Carbohydrate Polymers* **2009**, *77*, 420-424.
- (10) Kim, J.; Jia, H.; Wang, P. *Biotechnology Advances* **2006**, *24*, 296-308.
- (11) Moore, C. M.; Akers, N. L.; Hill, A. D.; Johnson, Z. C.; Minteer, S. D. *Biomacromolecules* **2004**, *5*, 1241-1247.
- (12) Dutta, P. K.; Ravikumar, M. N. V.; Dutta, J. *Journal of Macromolecular Science - Polymer Reviews* **2002**, *42*, 307-355.
- (13) Park, J. W.; Choi, K.-H.; Park, K. K. *Bulletin of Korean Chemical Society* **1983**, *4*, 68-72.
- (14) Wang, Q. Z.; Chen, X. G.; Liu, N.; Wang, S. X.; Liu, C. S.; Meng, X. H.; Liu, C. G. *Carbohydrate Polymers* **2006**, *65*, 194-201.
- (15) Esquenet, C.; Buhler, E. *Macromolecules* **2001**, *34*, 5287-5294.
- (16) Esquenet, C.; Terech, P.; Boue, F.; Buhler, E. *Langmuir* **2004**, *20*, 3583-3592.
- (17) Park, C. R.; Kim, Y. H.; Lee, K. Y.; Kwon, I. C. *American Chemical Society, Polymer Preprints, Division of Polymer Chemistry* **2000**, *41*, 377-378.
- (18) Chebotok, E.; Novikov, V.; Konovalova, I. *Russian Journal of Applied Chemistry* **2006**, *79*, 1162-1166.
- (19) No, H. K.; Cho, Y. I.; Kim, H. R.; Meyers, S. P. *Journal of Agricultural and Food Chemistry* **2000**, *48*, 2625-2627.
- (20) Philippova, O. E.; Volkov, E. V.; Sitnikova, N. L.; Khokhlov, A. R.; Desbrieres, J.; Rinaudo, M. *Biomacromolecules* **2001**, *2*, 483-490.
- (21) Li, G.; Zhuang, Y.; Mu, Q.; Wang, M.; Fang, Y. e. *Carbohydrate Polymers* **2008**, *72*, 60-66.
- (22) Zhang, C.; Ding, Y.; Yu, L.; Ping, Q. *Colloids and Surfaces B: Biointerfaces* **2007**, *55*, 192-199.
- (23) Horii, F.; Ikada, Y.; Sakurada, I. *Journal of Polymer Science* **1974**, *12*, 323-335.

- (24) Yuan, Z.; Burckel, B. D.; Atanassov, P.; Fan, H. *Journal of Materials Chemistry* **2006**, *16*, 4637-4641.
- (25) Kuncicky, D. M.; Prevo, B. G.; Velev, O. D. *Journal of Materials Chemistry* **2006**, *16*, 1207-1211.
- (26) Yuan, Z.; Petsev, D. N.; Prevo, B. G.; Velev, O. D.; Atanassov, P. *Langmuir* **2007**, *23*, 5498-5504.
- (27) Ashley, C. E.; Dunphy, D. R.; Jiang, Z.; Carnes, E. C.; Yuan, Z.; Petsev, D. N.; Atanassov, P. B.; Velev, O. D.; Sprung, M.; Wang, J.; Peabody, D. S.; Brinker, C. J. *Small* **2011**, *7*, 1043-1050.
- (28) Minoofar, P. N.; Dunn, B. S.; Zink, J. I. *Journal of the American Chemical Society* **2005**, *127*, 2656-2665.